INTERNATIONAL JOURNAL FOR NUMERICAL METHODS IN ENGINEERING, VOL. 39, 1265–1293 (1996)

A SINGLE-DOMAIN BOUNDARY ELEMENT METHOD FOR 3-D ELASTOSTATIC CRACK ANALYSIS USING CONTINUOUS ELEMENTS

A. YOUNG

Structural Materials Centre, X34 Building, Defence Research Agency, Farnborough, Hants GU14 6TD, U.K.

SUMMARY

A boundary element method is presented for single-domain analysis of cracked three-dimensional isotropic elastostatic solids. A numerical treatment for the hypersingular Boundary Integro-Differential Equation (BIDE) for displacement derivatives is described, in which continuous boundary elements may be used. Hadamard principal values of the hypersingular integrals arising in the formulation are evaluated using polar co-ordinates defined on the tangent planes at the source point, and the free term coefficients are calculated directly using a numerical technique. The forms of the Boundary Integral Equation (BIE) and the BIDE are considered for a source point on the coincident surfaces of a crack, and a scheme is given for defining the Traction Boundary Integral Equation TBIE so that it optimally incorporates the traction information deficient in its complementary partner, the BIE. Numerical results for some example mixed-mode crack problems are presented.

KEY WORDS: boundary element method; traction equation; continuous elements; three-dimensional fracture

1. INTRODUCTION

Boundary Integral Equations for displacement (BIE) and traction (TBIE) provide a natural and elegant theoretical approach for analysing linear elastic crack problems.[1,2] However, designing a boundary element method for computing numerical solutions to the TBIE is not straightforward, as there are considerable analytical and numerical difficulties to be overcome.[3] One strategy is to use discontinuous boundary elements.[4,5] These elements are less accurate and computationally more expensive than continuous elements, but most of the practical problems arising in the numerical treatment of the TBIE are bypassed. However, when applied to three-dimensional crack problems, the size of the numerical system of equations generated by the mesh of discontinuous elements is often prohibitively large. In order to use the boundary element method efficiently and accurately for general cracks, it is essential to design a numerical formulation that allows use of conventional continuous elements.

The BIE alone is not capable of considering general crack problems, except by use of subdomaining,[6] as it is deficient in certain information involving tractions on the crack surfaces. This missing information is present in the TBIE, which provides a means to determine solutions for the opening displacement of interior cracks, known as the displacement difference method.[7] A complete boundary solution for general crack problems is provided by the dual boundary element method,[4,5] which involves applying both the BIE and the TBIE at source points on the

CCC 0029–5981/96/081265–29

Received 6 September 1994
Received 15 March 1995

locus of the dual crack surfaces. The TBIE is constructed from the hypersingular Boundary Integro-Differential Equation (BIDE) for displacement derivatives. Application of the conventional boundary element method, using continuous elements, to the hypersingular TBIE fails due to the unsuitable representation of the surface displacement and traction.[8] Existence of the limiting forms of the hypersingular BIDE and TBIE for source points on the boundary requires satisfaction of certain continuity conditions involving traction and displacement derivatives. These conditions must be embodied in the displacement and traction on the boundary, if numerical solutions of the TBIE are to converge to the correct result. For the special case where the source is on a smooth part of the boundary, the conditions reduce to the requirement that surface derivatives of displacement should be continuous at the boundary source point.[3,9] Then, one way of proceeding is to use special elements, such as Overhauser elements, that implicitly incorporate continuity of surface derivatives of the boundary variables.[10] However, the condition that derivatives of displacement should be continuous between elements is not satisfactory for source points at corners.

A more direct attack on the problem of using continuous elements involves subtracting leading terms from series expansions for traction and displacement about the source point, thereby isolating the hypersingular parts of the TBIE. Integrals involving the subtracted terms can be assigned unique values of displacement derivatives at the source point, and then converted to non-singular line integrals over some part of the boundary by way of Stokes' theorem.[11,12] This regularization results in an equivalent non-singular TBIE, in which detailed consideration of the limiting case of source points on the boundary is unnecessary. Whereas this approach provides a promising basis for a numerical method for the TBIE, its implementation is not straightforward, especially for three-dimensional analysis, and the numerical method described in this paper is developed in terms of hypersingular integral equations.

The aim of the present approach is to develop a boundary element method for the TBIE that may be used effectively for all crack problems. The theory includes a detailed consideration of the form of the hypersingular BIDE in the vicinity of a boundary source point. Continuity conditions for surface variables in the BIDE at an arbitrary corner point are inferred, and a scheme is described for regularizing the displacement and traction on continuous elements local to the source point. Hadamard Principal Values (HPV) of the hypersingular integrals that arise in the BIDE are evaluated using polar co-ordinates defined on the tangent planes at the source point, and the free-term coefficients of displacement in the BIE and of displacement derivatives in the BIDE are calculated directly using a numerical technique. The forms of the dual boundary element equations are considered for a source point on the coincident surfaces of a crack, and a scheme is given for defining the TBIE such that it optimally incorporates the traction information deficient in its complementary partner, the BIE. Finally, some example mixed-mode crack problems are considered in order to demonstrate the capability of the present method.

2. DEFINITIONS AND BASIC CONCEPTS

Consider a homogeneous, isotropic, linear elastic solid V bounded by the closed surface S, and with tensile modulus E and Poisson's ratio ν. The structure is to be analysed in terms of rectangular Cartesian co-ordinates $\mathbf{x} \equiv (x_1, x_2, x_3)$, and the summation convention is assumed for repeated lower case subscripts, with roman indices 1, 2, 3 and greek indices 1, 2. Components of displacement and stress at points $\mathbf{x}$ in V are denoted by $u_i(\mathbf{x})$ and $\sigma_{ij}(\mathbf{x})$, and tractions $t_i(\mathbf{x}) \equiv \sigma_{ij}(\mathbf{x})n_j(\mathbf{x})$ exist at points $\mathbf{x}$ on the boundary S, where $n_j(\mathbf{x})$ denotes the unit vector in the outward normal direction. The intention is to develop boundary integral equations associated with a source point $\mathbf{x}^0$ located arbitrarily on the boundary S.

It is useful to define the relative position vector

$$\mathbf{r} \equiv (r_1, r_2, r_3) = \mathbf{x} - \mathbf{x}^0 \tag{1}$$

and the associated quantities

$$r^2 = \mathbf{r}\cdot\mathbf{r} = r_k r_k, \quad r_{,i} \equiv \frac{\partial r}{\partial x_i} = -\frac{\partial r}{\partial x_i^0} = r_i/r \tag{2}$$

In order to facilitate the analytical derivation of the integral equations, the following auxiliary surfaces are defined in terms of an infinitesimal sphere $r = \varepsilon$ surrounding the boundary source point $\mathbf{x}^0$: S_ε is the part of $r = \varepsilon$ confined by the planes tangent to S at $\mathbf{x}^0$; S_x is the part of S exterior to $r = \varepsilon$; S_* is the part of the sphere $r = \varepsilon$ that lies between S_x and S_ε. The regions S_ε, S_* and S_x together comprise a closed surface $S(\varepsilon)$, which approximates the surface S of the solid V but excludes $\mathbf{x}^0$. The surface S_* exists by virtue of the curvature of S_x at $\mathbf{x}^0$ and will give a negative contribution to $S(\varepsilon)$ if the boundary S is convex at $\mathbf{x}^0$. When the source point $\mathbf{x}^0$ is on two coincident surfaces of a crack, there exist two sets of regions S_ε and S_*. Figure 1 shows the parts of the surfaces S_ε, S_* and S_x associated with an individual smooth boundary element, which are denoted by δS_ε, δS_* and δS_x.

Define the following integral expressions involving the source point $\mathbf{x}^0$ and a general surface S

$$I_j(\mathbf{x}^0; S) \equiv \int_S \{T_{ij}(\mathbf{x}, \mathbf{x}^0)u_i(\mathbf{x}) - U_{ij}(\mathbf{x}, \mathbf{x}^0)t_i(\mathbf{x})\}\, dS(\mathbf{x}) \tag{3}$$

$$I_{jk}(\mathbf{x}^0; S) \equiv \frac{\partial}{\partial x_k^0} I_j(\mathbf{x}^0; S) = \int_S \{T_{ijk}(\mathbf{x}, \mathbf{x}^0)u_i(\mathbf{x}) - U_{ijk}(\mathbf{x}, \mathbf{x}^0)t_i(\mathbf{x})\}\, dS(\mathbf{x}) \tag{4}$$

The kernels $U_{ij}(\mathbf{x}, \mathbf{x}^0)$ and $T_{ij}(\mathbf{x}, \mathbf{x}^0)$ are chosen to be the singular fundamental solutions for i-components of displacement and traction at the point $\mathbf{x}$ on the locus of S due to a concentrated

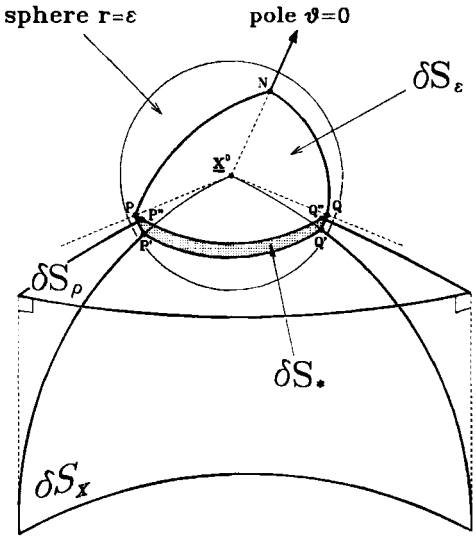

Figure 1. Contributions to the surfaces $S_\varepsilon(NPQ)$, $S_*(PP'Q'Q)$ and S_x from a curved element which includes the source point $\mathbf{x}^0$, and the associated projected tangent element δS_ρ

force acting in the j-direction at the point $\mathbf{x}^0$. These singular kernels for a three-dimensional isotropic solid are given by[13]

$$U_{ij}(\mathbf{x}, \mathbf{x}^0) = \frac{(1+\nu)r^{-1}}{8\pi(1-\nu)E}\{(3-4\nu)\delta_{ij} + r_{,i}r_{,j}\} \tag{5}$$

$$T_{ij}(\mathbf{x}, \mathbf{x}^0) = \frac{-r^{-2}}{8\pi(1-\nu)}\{[(1-2\nu)\delta_{ij} + 3r_{,i}r_{,j}]r_{,k}n_k + (1-2\nu)[r_{,i}n_j - r_{,j}n_i]\} \tag{6}$$

where $\delta_{ij} = 1$ if $i = j$ and $= 0$ otherwise. The related hypersingular kernels $U_{ijk}(\mathbf{x}, \mathbf{x}^0)$ and $T_{ijk}(\mathbf{x}, \mathbf{x}^0)$ are defined as

$$\begin{aligned} U_{ijk}(\mathbf{x}, \mathbf{x}^0) &\equiv \frac{\partial}{\partial x_k^0} U_{ij}(\mathbf{x}, \mathbf{x}^0) \\ &= \frac{(1+\nu)r^{-2}}{8\pi(1-\nu)E}\{3r_{,i}r_{,j}r_{,k} - \delta_{jk}r_{,i} - \delta_{ki}r_{,j} + (3-4\nu)\delta_{ij}r_{,k}\} \end{aligned} \tag{7}$$

$$\begin{aligned} T_{ijk}(\mathbf{x}, \mathbf{x}^0) &\equiv \frac{\partial}{\partial x_k^0} T_{ij}(\mathbf{x}, \mathbf{x}^0) \\ &= \frac{r^{-3}}{8\pi(1-\nu)}\{[3\delta_{jk}r_{,i} + 3\delta_{ki}r_{,j} - 3(1-2\nu)\delta_{ij}r_{,k} - 15r_{,i}r_{,j}r_{,k}]r_{,l}n_l \\ &\quad + [(1-2\nu)\delta_{ij} + 3r_{,i}r_{,j}]n_k - (1-2\nu)[\delta_{jk} - 3r_{,j}r_{,k}]n_i \\ &\quad + (1-2\nu)[\delta_{ki} - 3r_{,k}r_{,i}]n_j\} \end{aligned} \tag{8}$$

With the point $\mathbf{x}^0$ exterior to the surface $S(\varepsilon)$, the Boundary Integral Equation (BIE), or Somigliana's identity, is given by

$$I_j(\mathbf{x}^0; S(\varepsilon)) = 0 \tag{9}$$

The derivative of the BIE (9) with respect to the exterior source point coordinate x_k^0 is called the Boundary Integro-Differential Equation (BIDE),

$$I_{jk}(\mathbf{x}^0; S(\varepsilon)) = 0 \tag{10}$$

Equation (10) is the basis from which the TBIE for source points on the boundary surface S will be developed. By considering source points $\mathbf{x}^0$ exterior to the boundary $S(\varepsilon)$, a formulation results which is algebraically symmetric with respect to coincident crack surfaces.

As the radius of the spherical exclusion $r = \varepsilon$ is made vanishingly small, the auxiliary surface $S(\varepsilon)$ becomes equivalent to the surface S. If the boundary integral equations exist for a source point $\mathbf{x}^0$ on the surface S, then they will be equivalent to those for the limiting case $S(0) = \lim_{\varepsilon \to 0} S(\varepsilon)$. The limiting forms of the BIE and the BIDE for $\mathbf{x}^0$ not on a crack surface are

$$\begin{aligned} I_j(\mathbf{x}^0; S(0)) &= c_{ij}(\mathbf{x}^0)u_i(\mathbf{x}^0) \\ &\quad + \text{HPV}\int_S \{T_{ij}(\mathbf{x}, \mathbf{x}^0)u_i(\mathbf{x}) - U_{ij}(\mathbf{x}, \mathbf{x}^0)t_i(\mathbf{x})\}\, dS(\mathbf{x}) = 0 \end{aligned} \tag{11}$$

$$\begin{aligned} I_{kl}(\mathbf{x}^0; S(0)) &= C_{ijkl}(\mathbf{x}^0)u_{i,j}(\mathbf{x}^0) + d_{ikl}(\mathbf{x}^0)u_i(\mathbf{x}^0) \\ &\quad + \text{HPV}\int_S \{T_{ikl}(\mathbf{x}, \mathbf{x}^0)u_i(\mathbf{x}) - U_{ikl}(\mathbf{x}, \mathbf{x}^0)t_i(\mathbf{x})\}\, dS(\mathbf{x}) = 0 \end{aligned} \tag{12}$$

provided that certain continuity conditions are satisfied by the surface displacement and traction. When $\mathbf{x}^0$ is on a crack, equations (11) and (12) include two sets of free terms $c_{ij}(\mathbf{x}^0)u_i(\mathbf{x}^0)$ and $C_{ijkl}(\mathbf{x}^0)u_{i,j}(\mathbf{x}^0) + d_{ikl}(\mathbf{x}^0)u_i(\mathbf{x}^0)$ corresponding to contributions from each crack surface. For simplicity, the development of the BIE and the BIDE is described without a crack, and the important features for $\mathbf{x}^0$ on a crack are considered in Section 8.

The Hadamard principal values of the hypersingular integrals, denoted by HPV in equations (11) and (12), are special definitions arising from the artificial subdivision of the closed boundary $S(\varepsilon)$ into the surfaces S_ε, S_* and S_x. The integrals over the individual component surfaces involve ε^{-1} and $\log\varepsilon$ terms, which in the limit $\varepsilon \to 0$ become singular. However, the sum of these integrals represents the integral over the closed surface $S(\varepsilon)$, which by (9) and (10) is necessarily finite for all ε. No singularities actually exist provided that the displacement and traction fields satisfy certain continuity conditions on $S(\varepsilon)$ at the source point; these continuity conditions are addressed Section 3. The HPV is a notational device whereby the singular terms in the series expansion in ε of an improper integral are to be neglected, since they must ultimately cancel out when all such integrals are recombined, and it may be formally defined as the $O(1)$ term arising when a small symmetric neighbourhood of radius ε about the singular point is excluded from the domain of integration. All such integrals may be evaluated consistently by taking series expansions of the integrands in terms of radial distance from the singular point; the principal value is then the limit of the finite part of the integrated expansion, with all improper terms removed.

The conventional approach to numerically evaluating regular or weakly singular integrals over boundary elements is to use a local intrinsic coordinate system.[6,13] HPV integrals may also be processed using intrinsic co-ordinates,[3,5] although care must be taken to interpret the singular terms correctly and consistantly for all elements, since the region $r \leqslant \varepsilon$ is no longer symmetrical in the local intrinsic co-ordinate space. An alternative approach for HPV integrals is to use local polar co-ordinates defined on the planes tangent to each element at the source point. In this case, radial series expansions emerge automatically and the important ε^{-1} and $\log\varepsilon$ singular terms can be easily identified. The latter approach is used in the present method, where HPV integrals are to be evaluated numerically over each piecewise smooth surface element δS_x on S by reference to the projected vector $\boldsymbol{\rho} \equiv (\rho_1, \rho_2, \rho_3)$, defined by

$$\rho_i = r_i - (r_k n_k^0) n_i^0 \tag{13}$$

where $n_i^0 = n_i(\mathbf{x}^0)$ is the unit outward normal vector to the element at $\mathbf{x}^0$. The vector $\boldsymbol{\rho}$ is the projection of $\mathbf{r}$ on δS_x onto the plane δS_ρ tangent to the element at the source point $\mathbf{x}^0$ (see Figure 1). Hypersingular leading terms are separated from the integrands in the BIDE (12) and expressed in terms of polar co-ordinates on the tangent plane. The use of these local polar co-ordinates for integration provides a natural representation for the spherical exclusion of radius ε, and this consequently leads to a simple and consistent means of evaluating HPV integrals. This process requires the definition of series expansions for hypersingular integrands in terms of the tangent plane co-ordinates (ρ_1, ρ_2, ρ_3). Formulae concerning the geometry of the surface δS_x local to the source point and the numerical evaluation of certain important quantities required in the series expansions are given in the Appendix.

In the conventional numerical method[13-15] for solution of the BIE (11), the surface S is subdivided into several piecewise continuous isoparametric boundary elements, over each of which the co-ordinates are assumed to be of the form

$$x_i \equiv x_i(\boldsymbol{\xi}) \equiv \sum_m x_i^{(m)} N^{(m)}(\boldsymbol{\xi}) \tag{14}$$

and the surface variables $u_i(\mathbf{x})$ and $t_i(\mathbf{x})$ are represented similarly as

$$u_i(\mathbf{x}) \approx \bar{u}_i(\xi) \equiv \sum_m u_i^{(m)} N^{(m)}(\xi)$$
$$t_i(\mathbf{x}) \approx \bar{t}_i(\xi) \equiv \sum_m t_i^{(m)} N^{(m)}(\xi) \tag{15}$$

The parameters $u_i^{(m)}$, $t_i^{(m)}$ and $x_i^{(m)}$ form a discrete set of nodal values associated with the element, the intrinsic surface co-ordinates $\xi \equiv (\xi_1, \xi_2)$ are defined separately for each element, and $N^{(m)}(\xi)$ are polynomial interpolation functions with the property

$$N^{(m)}(\xi) = \begin{cases} 1 \text{ at node } m \\ 0 \text{ at other nodes} \end{cases} \tag{16}$$

on the element. The conventional boundary element method uses the assumed forms for the solution (15) over all elements in the BIE (11) to generate a set of simultaneous linear equations in the values of displacement $u_i^{(m)}$ and traction $t_i^{(m)}$ at all nodes, from source points $\mathbf{x}^0$ taken at the nodal positions. However, this approach is unsuitable as a numerical treatment of the hypersingular BIDE and the subsequent TBIE when source points are taken on the edges of boundary elements, and a special interpolation scheme must be used.

3. NUMERICAL TREATMENT OF THE HYPERSINGULAR BIDE

The singularities in the kernel functions $T_{ijk}(\mathbf{x}, \mathbf{x}^0)$ and $U_{ijk}(\mathbf{x}, \mathbf{x}^0)$ in the BIDE (10) are of a higher order than those in the BIE, and it is necessary to consider the assumed form of the solution $u_i(\mathbf{x})$ and $t_i(\mathbf{x})$ in more detail. On a continuous part of the surface $S(\varepsilon)$ near to the source point $\mathbf{x}^0$, any solution should be of the form

$$u_i(\mathbf{x}) = u_i^0 + u_{i,j}^0 r_j + O(r^2) \tag{17}$$
$$t_i(\mathbf{x}) = t_i^0 + O(r) \tag{18}$$

where $u_i^0 \equiv u_i(\mathbf{x}^0)$, $u_{i,j}^0 \equiv u_{i,j}(\mathbf{x}^0)$ and $t_i^0 \equiv t_i(\mathbf{x}^0)$ are all evaluated at the source point. It is assumed that the displacement $u_i(\mathbf{x})$ and its first derivatives $u_{i,j}(\mathbf{x})$ are continuous at the source point, so that u_i^0 and $u_{i,j}^0$ are single valued. Then, taking account of the form of the hypersingular kernels (7) and (8) on the surface S_x and on the sphere $r = \varepsilon$, the following contributions to the BIDE are obtained:

$$I_{kl}(\mathbf{x}^0; S_x; \varepsilon) = \varepsilon^{-1}[B_{ikl}(\mathbf{x}^0)u_i^0] + \log\varepsilon[\alpha_{ikl}(\mathbf{x}^0)u_i^0 + \beta_{ijkl}(\mathbf{x}^0)u_{i,j}^0 + \gamma_{ikl}(\mathbf{x}^0)t_i^0]$$
$$+ \text{HPV}\int_S \{T_{ikl}(\mathbf{x}, \mathbf{x}^0)u_i(\mathbf{x}) - U_{ikl}(\mathbf{x}, \mathbf{x}^0)t_i(\mathbf{x})\}\, dS(\mathbf{x}) + O(\varepsilon) \tag{19}$$

$$I_{kl}(\mathbf{x}^0; S_\varepsilon; \varepsilon) = \varepsilon^{-1}[\bar{B}_{ikl}(\mathbf{x}^0)u_i^0] + c_{ijkl}(\mathbf{x}^0)u_{i,j}^0 + O(\varepsilon) \tag{20}$$

$$I_{kl}(\mathbf{x}^0; S_*; \varepsilon) = d_{ikl}(\mathbf{x}^0)u_i^0 + O(\varepsilon) \tag{21}$$

the sum of which gives the left-hand side of the BIDE (10). In principle, Stokes' theorem may be used to convert the contributions to the BIDE from the surfaces S_ε, S_* and those elements δS_x when adjoin the source point into non-singular line integrals taken around the outer perimeter of the elements.[11,12] However, in the present analysis, these contributions are treated separately and the hypersingular nature of the integrals is retained.

If the field variables $u_i(\mathbf{x})$ and $t_i(\mathbf{x})$ constitute a valid elasticity solution, then they must satisfy the BIDE for all values of ε, and the coefficients of each term in the expansions of the decomposed integrals (19)–(21) must sum to zero. When approximate numerical solutions are sought in terms of polynomial interpolations over boundary elements, they will not necessarily satisfy the same conditions at the source point as an exact elasticity solution. For an interpolation scheme to be valid, it is imperative that the singular terms involving ε^{-1} and $\log\varepsilon$ cancel out exactly, otherwise the limit $\varepsilon \to 0$ of the BIDE cannot be taken. This is achieved by defining special interpolations for displacement and traction which incorporate the same continuity properties that allow this cancellation for an exact solution. Simply ignoring the singular terms is not satisfactory, and leads to an invalid numerical method in which nodal solutions do not converge for general problems.

In the BIDE, the coefficients of ε^{-1} involve only the numerical values of displacement at the source point. The only general physical condition involving u_i^0 alone that is satisfied by exact solutions is continuity. Therefore, the coefficients of ε^{-1} for an approximate solution must cancel out if the assumed form for the displacement is continuous at the source positions, and so the contributions from S_x and S_ε in (19) and (20) must satisfy $B_{ikl}(\mathbf{x}^0) + \bar{B}_{ikl}(\mathbf{x}^0) = 0$. The $\log\varepsilon$-singular terms arise only from the hypersingular integral over S_x, and represent linear combinations of displacement, traction and derivatives of displacement at the source point that should be zero for an exact solution. No general relationship exists connecting displacement with tractions or displacement derivatives evaluated at a single point. Therefore, the displacement term may be considered independently, and as for the coefficient of ε^{-1}, it may be inferred that $\alpha_{ikl}(\mathbf{x}^0)$ must be identically zero if the displacement on the surface S is continuous at the source point. The only candidates for the remaining combinations $\beta_{ijkl}(\mathbf{x}^0)u_{i,j}^0 + \gamma_{ikl}(\mathbf{x}^0)t_i^0$ that are identically zero for exact solutions are linear combinations of the equations that define traction, by way of stress and strain, in terms of displacement derivatives

$$t_i^0 - E_{ijkl}n_j^0 u_{k,l}^0 = 0 \tag{22}$$

where

$$E_{ijkl} = \frac{E}{2(1+\nu)}\left\{\delta_{ik}\delta_{jl} + \delta_{il}\delta_{jk} + \frac{2\nu}{1-2\nu}\delta_{ij}\delta_{kl}\right\} \tag{23}$$

and n_j^0 refers to the unit outward normal at $\mathbf{x}^0$ on the boundary element on which the traction t_i^0 is applied. Therefore, if displacement is continuous at the source point and tractions at the source point on each boundary element are related to the derivatives of displacement precisely as in the formula (22), then the coefficient of $\log\varepsilon$ in (19) must be identically zero. If the condition (22) is not satisfied by the interpolation scheme, then $\log\varepsilon$ singular terms will remain and the limit of the BIDE as $\varepsilon \to 0$ will be invalid. When $\mathbf{x}^0$ is on a crack, the requirement is that these continuity conditions should be satisfied on each of the crack surfaces individually. A special case arises for $\mathbf{x}^0$ on a smooth part of the boundary with single-valued tractions and tangential derivatives of displacement, when the coefficients of $\log\varepsilon$ are zero due to the antisymmetry of the hypersingular integrands on the unique tangent plane; this may be seen later from equations (33) and (34). This latter case results in a simpler formulation in which discontinuous boundary elements may be used.[5]

The elemental representations of displacement and traction (15) are suitable as approximations to the solution of the BIE (11). However, these representations are not suitable as approximations to the surface variables in the BIDE on an element that includes the source point, unless $\mathbf{x}^0$ lies inside the perimeter of the element, such as for discontinuous elements.[4,5] In the general case, there are singular $\log\varepsilon$ terms occurring in the BIDE that cancel out only if the tractions t_i^0 are

consistent with the displacement derivatives $u^0_{i,j}$ at the source point $\mathbf{x}^0$. This condition requires that the spatial derivatives of the assumed boundary displacement are single valued at the source point and that traction vectors on all elements at the source point are precisely of the form (22).

In view of this higher-order continuity requirement, a special interpolation scheme may be defined which satisfies (22) exactly. This interpolation explicitly incorporates unique values of displacement derivatives $u^0_{i,j}$ at $\mathbf{x}^0$, and its use results in the occurrence of extra terms involving $u^0_{i,j}$ in the contribution to the BIDE from S_x. Later, these extra terms are to be combined with the free terms $c_{ijkl}u^0_{i,j}$ obtained from the surface S_ε, and a TBIE will be defined in which the displacement derivatives are combined into traction values. The proposed special interpolation scheme is

$$u_i(\mathbf{x}) \approx \tilde{u}_i(\xi) \equiv \bar{u}_i(\xi) + \{u^0_{i,k} - \bar{u}_{i,k}(\xi^0)\}\rho_k \bar{N}(\xi) = u^0_i + u^0_{i,k} r_k + O(r^2) \tag{24}$$

$$t_i(\mathbf{x}) \approx \tilde{t}_i(\xi) \equiv \bar{t}_i(\xi) + \{E_{ijkl}n^0_j u^0_{k,l} - \bar{t}_i(\xi^0)\}\bar{N}(\xi) = E_{ijkl}n^0_j u^0_{k,l} + O(r) \tag{25}$$

and is to be used only on those elements δS_x that include the source point $\mathbf{x}^0 = \mathbf{x}(\xi^0)$ on their perimeters; the usual form of interpolation (15) is used on elements which do not include the source point and on elements which include the source point in their interiors. The first-order expansion terms.

$$\bar{u}_{i,k}(\xi^0)\rho_k = \left[\frac{\partial \bar{u}_i}{\partial x_k}\right]^0 \rho_k = \left[\frac{\partial \bar{u}_i}{\partial \rho_k}\right]^0 \rho_k = \sum_m u_i^{(m)} \left[\frac{\partial N^{(m)}}{\partial \rho_k}\right]^0 \rho_k \tag{26}$$

are evaluated numerically using the formula (111) in the Appendix.

The factor $\bar{N}(\xi)$ may be any function of position on the element that satisfies

$$\bar{N}(\xi) = \begin{cases} 1 & \text{at the source point } \xi = \xi^0 \\ 0 & \text{on element edges that do not include } \xi = \xi^0 \end{cases} \tag{27}$$

provided that such functions are continuous between elements. Equations (24) and (25) define an infinite set of possible interpolations depending upon the choice of $\bar{N}(\xi)$, which is arbitrary apart from the constraints mentioned above. When the source point coincides with one of the nodes on the element, the factor $\bar{N}(\xi)$ may be taken to be the interpolation function (16) associated with the source node. Other possibilities include the interpolation function (16) raised to an integer power, and some comments concerning the influence of $\bar{N}(\xi)$ on numerical solutions of the TBIE are given later in Section 10. The reason for including the factor $\bar{N}(\xi)$ in (24) and (25) is to ensure that the effects of regularizing the displacement and traction are restricted to the boundary elements local to the source position.

The special representation of displacement $\tilde{u}_i(\xi)$ in (24) gives a smooth interpolation between the nodal values $u_i^{(m)}$ on an element, and incorporates first derivatives $\tilde{u}_{i,k}(\xi^0) = u^0_{i,k}$ at the source point which are independent of the nodal displacements and which may therefore be defined uniquely on all adjoining elements. The special form for the traction $\tilde{t}_i(\xi)$ in (25) gives an interpolation between the nodal values $t_i^{(m)}$ on the element, except for the source node where $\tilde{t}_i(\xi^0)$ at $\mathbf{x}^0$ on all elements is replaced by $E_{ijkl}n^0_j u^0_{k,l}$ as required by (22). In this way, using $\tilde{u}_i(\xi)$ and $\tilde{t}_i(\xi)$ local to the source point ensures cancellation of the $\log \varepsilon$-singular term (19) in the BIDE. Notice that the special interpolations (24) and (25) depend upon the position of the source, and that different interpolations are to be used depending upon whether or not a given element contains the source point. Although this inconsistency in unorthodox, numerical solutions in the form of discrete sets of nodal displacement and traction values converge satisfactorily to the correct result.

When the BIDE is used as a basis for a boundary element method, the HPV integrals must be evaluated numerically. A simple way to be do this on a given curved element δS_x is to use polar co-ordinates ρ (radius) and ψ (angle) defined in the tangent plane δS_ρ at $\mathbf{x}^0$. The integrands are expanded in powers of the polar radius ρ and the leading hypersingular terms are integrated separately. Expansions for r_i and n_i in terms of ρ and ψ are given by (101) and (103) in the Appendix, and when substituted into the kernels (7) and (8), give

$$T_{ijk}(\mathbf{x}, \mathbf{x}^0) = \rho^{-3} T^{(3)}_{ijk}(\psi) + \rho^{-2} T^{(2)}_{ijk}(\psi) + O(r^{-1}) \tag{28}$$

$$U_{ijk}(\mathbf{x}, \mathbf{x}^0) = \rho^{-2} U^{(2)}_{ijk}(\psi) + O(r^{-1}) \tag{29}$$

where

$$T^{(3)}_{ijk}(\psi) = \frac{1}{8\pi(1-\nu)}\{[(1-2\nu)\delta_{ij} + 3\rho_{,i}\rho_{,j}]n^0_k - (1-2\nu)[\delta_{jk} - 3\rho_{,j}\rho_{,k}]n^0_i + (1-2\nu)[\delta_{ki} - 3\rho_{,k}\rho_{,i}]n^0_j\} \tag{30}$$

$$T^{(2)}_{ijk}(\psi) = \frac{\kappa(\psi)}{16\pi(1-\nu)}\{9\rho_{,i}\rho_{,j}\rho_{,k} + 4n^0_i\rho_{,j}n^0_k + 2\rho_{,i}n^0_j n^0_k + (1-2\nu)\delta_{ij}\rho_{,k} - 5\delta_{jk}\rho_{,i} + (5-6\nu)\delta_{ki}\rho_{,j}\} \tag{31}$$

$$U^{(2)}_{ijk}(\psi) = \frac{(1+\nu)}{8\pi(1-\nu)E}\{3\rho_{,i}\rho_{,j}\rho_{,k} - \delta_{jk}\rho_{,i} - \delta_{ki}\rho_{,j} + (3-4\nu)\delta_{ij}\rho_{,k}\} \tag{32}$$

$\rho_{,i} = \rho_i/\rho$ are components of a unit vector in the direction of the polar angle ψ, and $\kappa(\psi)$ is the curvature of the surface δS_x at $\mathbf{x}^0$ in the direction of ψ, arising from (104) and calculated using (114). Using the assumed forms (24) and (25) for displacement and traction on the element, the integrands in the BIDE over δS_x are then of the form

$$T_{ijk}(\mathbf{x}, \mathbf{x}^0)\tilde{u}_i(\mathbf{x}) = \rho^{-3} T^{(3)}_{ijk}(\psi)u^0_i + \rho^{-2}\{T^{(2)}_{ijk}(\psi)u^0_i + T^{(3)}_{ijk}(\psi)\rho_{,l}u^0_{i,l}\} + O(r^{-1}) \tag{33}$$

$$U_{ijk}(\mathbf{x}, \mathbf{x}^0)\tilde{t}_i(\mathbf{x}) = \rho^{-2} U^{(2)}_{ijk}(\psi)(E_{impq}n^0_m u^0_{p,q}) + O(r^{-1}) \tag{34}$$

where the coefficients of ρ^{-3} and ρ^{-2} are functions of the plane polar angle ψ only. Integration of the hypersingular terms (33) and (34) over S_x, with $\rho \geqslant \varepsilon$, gives the expression involving ε^{-1} and $\log\varepsilon$ seen earlier in (19).

The differential area on the element δS_x is of the form

$$\mathrm{d}S(\mathbf{x}) = J(\mathbf{x}; \xi)\,\mathrm{d}\xi_1\,\mathrm{d}\xi_2 \tag{35}$$

where

$$\frac{\partial \mathbf{x}}{\partial \xi_1} \times \frac{\partial \mathbf{x}}{\partial \xi_2} = J(\mathbf{x}; \xi)\mathbf{n} \tag{36}$$

and $\mathbf{n}$ is the unit outward normal to δS_x at $\mathbf{x}$. The corresponding differential area on the tangent plane δS_ρ is

$$\mathrm{d}S(\boldsymbol{\rho}) = J(\boldsymbol{\rho}; \xi)\,\mathrm{d}\xi_1\,\mathrm{d}\xi_2 \tag{37}$$

where the Jacobians $J(\mathbf{x}; \xi)$ and $J(\boldsymbol{\rho}; \xi)$ are related by

$$J(\boldsymbol{\rho}; \xi) = \frac{\partial \boldsymbol{\rho}}{\partial \xi_1} \times \frac{\partial \boldsymbol{\rho}}{\partial \xi_2} \cdot \mathbf{n}^0 = \frac{\partial \mathbf{x}}{\partial \xi_1} \times \frac{\partial \mathbf{x}}{\partial \xi_2} \cdot \mathbf{n}^0 = J(\mathbf{x}; \xi)\mathbf{n} \cdot \mathbf{n}^0 \tag{38}$$

and $\mathbf{n}\cdot\mathbf{n}^0 = 1 + O(\rho^2)$ from (103). An alternative form of the tangent differential area in plane polar co-ordinates is

$$dS(\boldsymbol{\rho}) = \rho\, d\rho\, d\psi \tag{39}$$

and this is the form to be used to evaluate the HPV integrals.

Upon substituting the series expansions (24) and (25) into the the contribution to the BIDE from δS_x (19), the integrals over those elements that include the source point $\mathbf{x}^0$ are of the form

$$\begin{aligned}
\text{HPV}\int_{\delta S_x} T_{ijk}(\mathbf{x},\mathbf{x}^0)\tilde{u}_i(\mathbf{x})\,dS(\mathbf{x}) = &\int_{\delta S_x}\{T_{ijk}(\mathbf{x},\mathbf{x}^0)\tilde{u}_i(\mathbf{x})\\
&-(\mathbf{n}\cdot\mathbf{n}^0)\{(\rho^{-3}T^{(3)}_{ijk}(\psi)+\rho^{-2}T^{(2)}_{ijk}(\psi))u^0_i+\rho^{-2}T^{(3)}_{ijk}(\psi)\rho_{,l}u^0_{i,l}\}\}\,dS(\mathbf{x})\\
&+u^0_i\,\text{HPV}\int_{\delta S_\rho}(\rho^{-3}T^{(3)}_{ijk}(\psi)+\rho^{-2}T^{(2)}_{ijk}(\psi))\,dS(\boldsymbol{\rho})\\
&+u^0_{i,l}\,\text{HPV}\int_{\delta S_\rho}\rho^{-2}T^{(3)}_{ijk}(\psi)\rho_{,l}(\psi)\,dS(\boldsymbol{\rho})
\end{aligned} \tag{40}$$

$$\begin{aligned}
\text{HPV}\int_{\delta S_x} U_{ijk}(\mathbf{x},\mathbf{x}^0)\tilde{t}_i(\mathbf{x})\,dS(\mathbf{x}) = &\int_{\delta S_x}\{U_{ijk}(\mathbf{x},\mathbf{x}^0)\tilde{t}_i(\mathbf{x})\\
&-(\mathbf{n}\cdot\mathbf{n}^0)\{\rho^{-2}U^{(2)}_{ijk}(\psi)E_{impq}n^0_m u^0_{p,q}\}\}\,dS(\mathbf{x})\\
&+E_{impq}n^0_m u^0_{p,q}\,\text{HPV}\int_{\delta S_\rho}\rho^{-2}U^{(2)}_{ijk}(\psi)\,dS(\boldsymbol{\rho})
\end{aligned} \tag{41}$$

Thus the contribution to the BIDE from S_x involves displacement and traction variables on the surface S, along with the displacement derivatives $u^0_{i,j}$ at the source point introduced by way of (24) and (25). When the contributions to the BIDE from the surfaces S_x and S_ε are recombined, any terms involving the displacement derivatives $u^0_{i,j}$ are to be grouped together and ultimately reduced to expressions involving traction values at the source point.

4. NUMERICAL EVALUATION OF HPV INTEGRALS

The HPV integrals, (40) and (41), arising in the BIDE over a curved element δS_x that includes the source point are of the form

$$\text{HPV}\int_{\delta S_x}\frac{1}{r^\alpha}f(\hat{\mathbf{r}})\,dS(\mathbf{x}) = \int_{\delta S_x}\left\{\frac{1}{r^\alpha}f(\hat{\mathbf{r}})-\frac{\mathbf{n}\cdot\mathbf{n}_0}{\rho^\alpha}f(\hat{\boldsymbol{\rho}})\right\}dS(\mathbf{x})+\text{HPV}\int_{\delta S_\rho}\frac{1}{\rho^\alpha}f(\hat{\boldsymbol{\rho}})\,dS(\boldsymbol{\rho}) \tag{42}$$

where $\alpha = 2$ or 3, $\hat{\mathbf{r}} \equiv \mathbf{r}/r$ and $\hat{\boldsymbol{\rho}} \equiv \boldsymbol{\rho}/\rho$ are unit vectors, and $\mathbf{n}\cdot\mathbf{n}_0 = 1 + O(\rho^2)$. The integral over δS_x on the right-hand side is not singular and may be evaluated using the usual methods for $O(r^{-1})$ integrands.[15,16] The HPV integral over the plane projected element δS_ρ on the right-hand side of (42) is to be evaluated in terms of the polar co-ordinates ρ and ψ, where $dS(\boldsymbol{\rho}) = \mathbf{n}\cdot\mathbf{n}_0\,dS(\mathbf{x}) = \rho\,d\rho\,d\psi$.

Integration with respect to the radial co-ordinate ρ is performed analytically over $\varepsilon \leqslant \rho \leqslant \bar{\rho}(\psi)$, resulting in a line integral with respect to the angular co-ordinate ψ taken around the perimeter of the projected element δS_ρ. The angular variable ψ is represented in terms of an intrinsic parameter $-1 \leqslant \eta \leqslant +1$ defined along each piecewise smooth edge of δS_ρ. Then, the HPV

integral on the right-hand side of (42) is to be interpreted as the $O(1)$ term arising from the series expansion in ε of

$$\sum_{\text{edges}} \int_{\psi(-1)}^{\psi(+1)} \int_{\varepsilon}^{\bar{\rho}(\psi)} \frac{1}{\rho^{\alpha}} f(\hat{\mathbf{p}}(\psi))\, \rho \, \mathrm{d}\rho \, \mathrm{d}\psi = \sum_{\text{edges}} \int_{-1}^{+1} \left[\int_{\varepsilon}^{\bar{\rho}(\psi)} \frac{\mathrm{d}\rho}{\rho^{\alpha-1}} \right] f(\hat{\mathbf{p}}(\psi(\eta)))\psi'(\eta)\,\mathrm{d}\eta \tag{43}$$

where $\psi'(\eta) = \mathrm{d}\psi/\mathrm{d}\eta$, and

$$\begin{aligned} \int_{\varepsilon}^{\bar{\rho}(\psi)} \frac{\mathrm{d}\rho}{\rho} &= \log \bar{\rho}(\psi) - \log \varepsilon \\ \int_{\varepsilon}^{\bar{\rho}(\psi)} \frac{\mathrm{d}\rho}{\rho^2} &= \varepsilon^{-1} - (\bar{\rho}(\psi))^{-1} \end{aligned} \tag{44}$$

Then the area integral (43) reduces to a sum of line integrals over each continuous smooth edge section $\rho = \bar{\rho}(\psi)$ of the projected element δS_{ρ}. Each line integral may be considered in the form

$$\int_{\bar{\psi}_1(\varepsilon)}^{\psi_2} g(\bar{\rho}(\psi)) f(\hat{\mathbf{p}}(\psi))\,\mathrm{d}\psi - \int_{\bar{\psi}_1(\varepsilon)}^{\psi_2} g(\varepsilon) f(\hat{\mathbf{p}}(\psi))\,\mathrm{d}\psi \tag{45}$$

where $g(\rho) = \log \rho$ or $-\rho^{-1}$, and the lower limit of integration $\bar{\psi}_1(\varepsilon)$ depends on ε if the line edge is curved and meets the source point, as illustrated in Figure 2 and by the points P'' and Q'' in Figure 1.

On an edge section that does not include the source point, the HPV is obtained simply by omitting the singular term $g(\varepsilon)$ from (45) and setting $\varepsilon = 0$, thereby leaving a regular line integral. However, the case where (45) is to be evaluated over an edge section $\rho = \bar{\rho}(\psi)$ which is curved and which includes the source point at one end $\psi = \psi_1$, where $\bar{\rho}(\psi_1) = 0$, requires further attention. The line edge $\rho = \bar{\rho}(\psi)$ intersects the sphere $r = \varepsilon$ at the angle

$$\bar{\psi}_1(\varepsilon) = \psi_1 + \bar{\kappa}\varepsilon + O(\varepsilon^2) \tag{46}$$

where $\psi = \psi_1$ is tangent to the line edge at the source point and $\bar{\kappa} = (\bar{\rho}'(\psi_1))^{-1}$ is the curvature of the line edge at the source point. Note that the curvature parameter $\bar{\kappa}$ is due to the shape of the

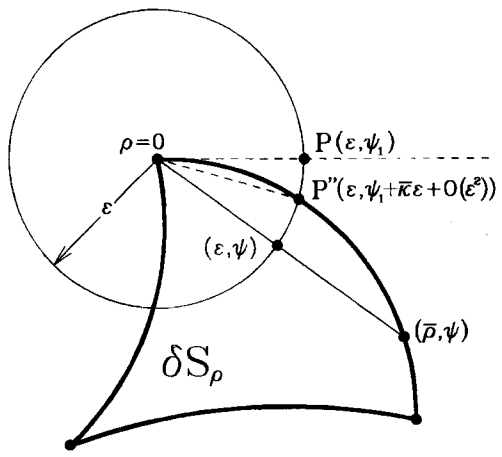

Figure 2. Plane projected element δS_{ρ} and the associated polar co-ordinates (ρ, ψ), showing the intersection P'' of a curved edge with the sphere $r = \varepsilon$

projected element δS_ρ, and is not the same as the intrinsic curvature $\kappa(\psi)$ of the surface δS_x occurring in (101) and (31). The first integral in (45) involves a singular integrand $g(\bar{\rho}(\bar{\psi}_1(\varepsilon))) = \log\varepsilon$ or $-\varepsilon^{-1}$, and so it must be interpreted consistently with the definition of HPV as the $O(1)$ term from a series expansion in the radius ε. The HPV integrals with respect to the angle ψ may be considered using a change of variable to the quasi-radial distance $\rho^*(\psi)$ defined by

$$\begin{aligned} \rho^*(\psi) &\equiv \bar{\rho}'(\psi_1)(\psi - \psi_1) \\ \psi(\rho^*) &\equiv \psi_1 + \bar{\kappa}\rho^* \end{aligned} \tag{47}$$

Near to the source point $\psi = \psi_1$, $\bar{\rho} = \rho^* + O(\rho^{*2})$ and so

$$\begin{aligned} \log\bar{\rho} &= \log\rho^* + O(\rho^*) \\ (\bar{\rho})^{-1} &= (\rho^*)^{-1} + O(1) \end{aligned} \tag{48}$$

The lower limit of integration corresponds to $\rho^*(\bar{\psi}_1(\varepsilon)) \equiv \varepsilon + O(\varepsilon^2)$ and so

$$\begin{aligned} \int_{\bar{\psi}_1(\varepsilon)}^{\psi_2} g(\bar{\rho}(\psi))f(\hat{\mathbf{p}}(\psi))\,\mathrm{d}\psi &= \int_{\varepsilon}^{\rho(\psi_2)} g(\bar{\rho}(\psi(\rho^*)))f(\hat{\mathbf{p}}(\psi(\rho^*)))\bar{\kappa}\,\mathrm{d}\rho^* + O(\varepsilon) \\ &= \bar{\kappa}\int_{\varepsilon}^{\rho^*(\psi_2)} \{g(\bar{\rho}(\psi(\rho^*)))f(\hat{\mathbf{p}}(\psi(\rho^*))) - g(\rho^*)f(\hat{\mathbf{p}}(\psi_1))\}\,\mathrm{d}\rho^* \\ &\quad + \bar{\kappa}f(\hat{\mathbf{p}}(\psi_1))\int_{\varepsilon}^{\rho^*(\psi_2)} g(\rho^*)\,\mathrm{d}\rho^* + O(\varepsilon) \end{aligned} \tag{49}$$

where $\hat{\mathbf{p}}(\psi_1) = \lim_{\psi\to\psi_1}\hat{\mathbf{p}}(\psi)$ is a unit vector tangent to the edge section at the source point. Owing to (48), the first integral on the right-hand side of (49) is regular. The second integral on the right-hand side is not singular for the integrand $g(\rho^*) = \log\rho^*$, but it is singular for $g(\rho^*) = -(\rho^*)^{-1}$ and must then be evaluated as a HPV. As $\varepsilon\to 0$, the finite part of (49) reduces to

$$\begin{aligned} \mathrm{HPV}\int_{\psi_1}^{\psi_2} g(\bar{\rho}(\psi))f(\hat{\mathbf{p}}(\psi))\,\mathrm{d}\psi &= \int_{\psi_1}^{\psi_2} \{g(\bar{\rho}(\psi))f(\hat{\mathbf{p}}(\psi)) - g(\rho^*(\psi))f(\hat{\mathbf{p}}(\psi_1))\}\,\mathrm{d}\psi \\ &\quad + \bar{\kappa}f(\hat{\mathbf{p}}(\psi_1))\,\mathrm{HPV}\int_0^{\rho^*(\psi_2)} g(\rho^*)\,\mathrm{d}\rho^* \end{aligned} \tag{50}$$

where

$$\begin{aligned} \mathrm{HPV}\left\{\int_0^{\rho^*}\log\rho^*\,\mathrm{d}\rho^*\right\} &= \int_0^{\rho^*}\log\rho^*\,\mathrm{d}\rho^* = \rho^*\log\rho^* - \rho^* \\ \mathrm{HPV}\left\{\int_0^{\rho^*}\frac{\mathrm{d}\rho^*}{\rho^*}\right\} &= \log\rho^* \end{aligned} \tag{51}$$

In order to evaluate the limit as $\varepsilon\to 0$ of the second integral in (45) consistently with the definition of HPV, it is expressed as a series expansion in the radius ε. Since

$$\lim_{\varepsilon\to 0}\frac{1}{\varepsilon}\int_{\psi_1}^{\psi_1+\bar{\kappa}\varepsilon} f(\psi)\,\mathrm{d}\psi = \bar{\kappa}f(\psi_1) \tag{52}$$

the second integral is of the form

$$\int_{\bar{\psi}_1(\varepsilon)}^{\psi_2} g(\varepsilon) f(\hat{\boldsymbol{\rho}}(\psi))\,\mathrm{d}\psi = \int_{\psi_1}^{\psi_2} g(\varepsilon) f(\hat{\boldsymbol{\rho}}(\psi))\,\mathrm{d}\psi - \int_{\psi_1}^{\psi_1+\bar{\kappa}\varepsilon+O(\varepsilon^2)} g(\varepsilon) f(\hat{\boldsymbol{\rho}}(\psi))\,\mathrm{d}\psi$$

$$= g(\varepsilon)\int_{\psi_1}^{\psi_2} f(\hat{\boldsymbol{\rho}}(\psi))\,\mathrm{d}\psi - g(\varepsilon)\{\varepsilon\bar{\kappa} f(\hat{\boldsymbol{\rho}}(\psi_1)) + O(\varepsilon^2)\} \tag{53}$$

The first term on the right-hand side of (53) is singular and will be omitted from the HPV. For $g(\varepsilon) = \log\varepsilon$, the remaining terms vanish as $\varepsilon \to 0$, while for $g(\varepsilon) = -\varepsilon^{-1}$, the remaining terms are $O(1)$. Then, as $\varepsilon \to 0$, the finite parts of the integrals (53) reduce to

$$\begin{aligned} &\mathrm{HPV}\lim_{\varepsilon\to 0}\left\{\log\varepsilon\int_{\psi_1(\varepsilon)}^{\psi_2} f(\hat{\boldsymbol{\rho}}(\psi))\,\mathrm{d}\psi\right\} = 0 \\ &\mathrm{HPV}\lim_{\varepsilon\to 0}\left\{-\varepsilon^{-1}\int_{\psi_1(\varepsilon)}^{\psi_2} f(\hat{\boldsymbol{\rho}}(\psi))\,\mathrm{d}\psi\right\} = \bar{\kappa} f(\hat{\boldsymbol{\rho}}(\psi_1)) \end{aligned} \tag{54}$$

Finally, after combining (45), (50) and (54) and using (47), the following formulae are obtained for evaluating the HPV integral on the right-hand side of (42):

$$\mathrm{HPV}\int_{\delta S_\rho} \frac{1}{\rho^\alpha} f(\hat{\boldsymbol{\rho}})\,\mathrm{d}S(\boldsymbol{\rho}) = \sum_{\text{edges}} I(\alpha) \tag{55}$$

where $I(\alpha)$ are evaluated over each continuous smooth edge section of δS_ρ using either

$$I(2) = \int_{-1}^{+1} \log(\bar{\rho}(\psi(\eta)))f(\hat{\boldsymbol{\rho}}(\psi(\eta)))\psi'(\eta)\mathrm{d}\eta \tag{56}$$

$$I(3) = \int_{-1}^{+1} -(\bar{\rho}(\psi(\eta)))^{-1} f(\hat{\boldsymbol{\rho}}(\psi(\eta)))\psi'(\eta)\,\mathrm{d}\eta \tag{57}$$

when the edge does not include the source point, or

$$\begin{aligned} I(2) = &\int_{-1}^{+1} \{\log(\bar{\rho}(\psi(\eta)))f(\hat{\boldsymbol{\rho}}(\psi(\eta))) - \log(\rho^*(\psi(\eta)))\, f(\hat{\boldsymbol{\rho}}(\psi_1))\}\psi'(\eta)\,\mathrm{d}\eta \\ &+ (\psi_2-\psi_1)[\log(\psi_2-\psi_1) - \log\bar{\kappa} - 1] f(\hat{\boldsymbol{\rho}}(\psi_1)) \end{aligned} \tag{58}$$

$$\begin{aligned} I(3) = &\int_{-1}^{+1} \{-(\bar{\rho}(\psi(\eta)))^{-1} f(\hat{\boldsymbol{\rho}}(\psi(\eta))) + (\rho^*(\psi(\eta)))^{-1}\, f(\hat{\boldsymbol{\rho}}(\psi_1))\}\psi'(\eta)\,\mathrm{d}\eta \\ &- \bar{\kappa}[\log(\psi_2-\psi_1) - \log\bar{\kappa} + 1] f(\hat{\boldsymbol{\rho}}(\psi_1)) \end{aligned} \tag{59}$$

when the edge includes the source at the end point $\psi = \psi_1$.

5. CALCULATION OF FREE-TERM COEFFICIENTS

This section describes a numerical method for calculating the free-term coefficients $c_{ijkl}(\mathbf{x}^0)$ arising in the hypersingular BIDE (12) due to the contribution from the surface S_ε. Although calculation of such terms may often be avoided by exploiting known reference solutions such as rigid-body translation,[13] consideration of coincident crack surfaces requires a direct evaluation. Expressions for the free-term coefficients $c_{ij}(\mathbf{x}^0)$ occurring in the BIE have been obtained in

closed form,[17] but no corresponding solution is yet available for the coefficients occurring in the BIDE.

On S_ε, the relative spatial co-ordinates take the form $r_i = -\varepsilon n_i$, where $\mathbf{n}$ is the unit outward normal to the surface $S(\varepsilon)$ at position $\mathbf{r} = \mathbf{x} - \mathbf{x}^0$. Assuming that the displacement derivatives are unique and consistent with the surface tractions, then the displacement and traction near $\mathbf{x}^0$ are of the form

$$u_i(\mathbf{x}) = u_i^0 - \varepsilon u_{i,j}^0 n_j(\mathbf{x}^0) + O(\varepsilon^2) \tag{60}$$

$$t_i(\mathbf{x}) = -E_{ijkl} u_{k,l}^0 n_j(\mathbf{x}^0) + O(\varepsilon) \tag{61}$$

where the elastic constants E_{ijkl} are as defined in (23). The kernel functions in the BIDE reduce to

$$T_{ijk}(\mathbf{x}, \mathbf{x}^0) = \varepsilon^{-3} \hat{T}_{ijk}(\mathbf{n})$$

$$\equiv \frac{\varepsilon^{-3}}{4\pi(1-\nu)} \{6n_i n_j n_k + (1-2\nu)\delta_{ij} n_k - (1+\nu)\delta_{jk} n_i - (2-\nu)\delta_{ki} n_j\} \tag{62}$$

$$U_{ijk}(\mathbf{x}, \mathbf{x}^0) = \varepsilon^{-2} \hat{U}_{ijk}(\mathbf{n})$$

$$\equiv \frac{(1+\nu)\varepsilon^{-2}}{8\pi(1-\nu)E} \{3n_i n_j n_k + (3-4\nu)\delta_{ij} n_k - \delta_{jk} n_i - \delta_{ki} n_j\} \tag{63}$$

and the integral (4) over S_ε reduces to the form (20), where the ε^{-1}-singular term cancels with a corresponding term from S_x.

In order to evaluate integrals over S_ε, define a set of local rectangular Cartesian co-ordinates $y \equiv (y_1, y_2, y_3)$ centred on $\mathbf{x}^0$, and a corresponding set of spherical polar co-ordinates (r, θ, ϕ) such that the positive y_3-axis coincides with the pole $\theta = 0$, the positive y_1-axis lies in the plane $\phi = 0$ and the positive y_2-axis lies in the plane $\phi = \pi/2$, as shown in Figure 3. Then the local Cartesian and polar co-ordinates are related by $y_1 = r\sin\theta\cos\phi$, $y_2 = r\sin\theta\sin\phi$ and $y_3 = r\cos\theta$. The surface S_ε is to include the co-ordinate pole $\theta = 0$ and to exclude the pole $\theta = \pi$, and this may be achieved if the negative y_3-direction $\theta = \pi$ corresponds to the average outward normal to the surface S at the source point $\mathbf{x}^0$; specifically, if the surface element $\delta S^{(e)}$ with outward unit normal vector $\mathbf{n}^{(e)}$ subtends a surface angle $\psi^{(e)}$ at $\mathbf{x}^0$, then the average outward

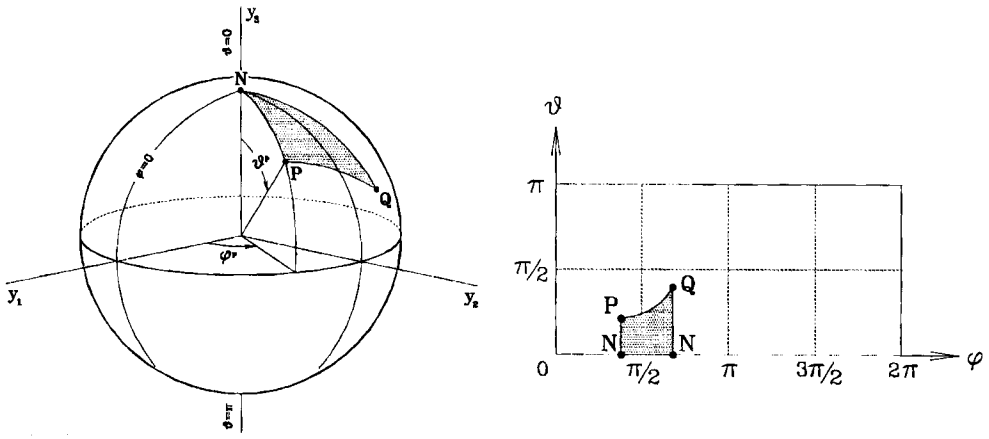

Figure 3. Spherical triangle NPQ on the infinitesimal surface S_ε, and its corresponding quadrilateral integration domain in (θ, ϕ) co-ordinates

normal direction $\theta = \pi$ is defined by $\sum \psi^{(e)} \mathbf{n}^{(e)}$. The half-plane $\phi = 0$ is chosen arbitrarily to contain any one of the element edge vectors $\mathbf{p}^{(e)}$, $\mathbf{q}^{(e)}$ at $\mathbf{x}^0$, and this is sufficient to define the local co-ordinate systems (y_1, y_2, y_3) and (r, θ, ϕ).

The accumulated list of edge vectors $\mathbf{p}^{(e)}$, $\mathbf{q}^{(e)}$ in (x_1, x_2, x_3) co-ordinates may be expressed in (y_1, y_2, y_3) co-ordinates using the rotation matrix R_{ij}

$$y_i = R_{ij} r_j \tag{64}$$

If the mutually orthogonal y_i-co-ordinate directions defined in (x_1, x_2, x_3) co-ordinates are used to construct three orthonormal vectors $\hat{\mathbf{r}}^{(i)}$, then $R_{ij} = \hat{r}_i^{(j)}$ by virtue of $R_{ij} R_{ik} = \delta_{jk}$. Similarly, the normal vector $\mathbf{n} = (n_1, n_3, n_3)$ in (x_1, x_2, x_3) co-ordinates may be expressed as $\mathbf{m} = (m_1, m_3, m_3)$ in (y_1, y_2, y_3) co-ordinates by $m_i = R_{ij} n_j$ or $n_j = R_{ij} m_i$. In terms of the spherical polar co-ordinate system defined above, the unit normal vector to the surface S_ε is $(m_1, m_2, m_3) = (-\sin\theta\cos\phi, -\sin\theta\sin\phi, -\cos\theta)$ and the differential area on S_ε is of the form $\mathrm{d}S(\mathbf{x}) = \varepsilon^2 \sin\theta \,\mathrm{d}\theta \,\mathrm{d}\phi$.

Then, the free term coefficients $c_{ijkl}(\mathbf{x}^0)$ in the BIDE are obtained using (60)–(63) in equations (4) and (20) and this gives

$$c_{ijkl}(\mathbf{x}^0) = R_{ai} R_{bj} R_{ck} R_{dl} \int_{S_\varepsilon} \{E_{ghab} m_h \hat{U}_{gcd}(\mathbf{m}) - m_b \hat{T}_{acd}(\mathbf{m})\} \sin\theta \,\mathrm{d}\theta \,\mathrm{d}\phi \tag{65}$$

Similarly, the coefficients $c_{ij}(\mathbf{x}^0)$ in the BIE (11) are

$$c_{ij}(\mathbf{x}^0) = \frac{R_{ki} R_{lj}}{8\pi(1-\nu)} \int_{S_\varepsilon} \{(1-2\nu)\delta_{kl} + 3m_k m_l\} \sin\theta \,\mathrm{d}\theta \,\mathrm{d}\phi \tag{66}$$

If $\mathbf{x}^0$ lies on a smooth part of the boundary S, such as the interior of a boundary element, then the domain of integration is $\{0 \leqslant \theta \leqslant \pi/2;\ 0 \leqslant \phi \leqslant 2\pi\}$ and the above formulae reduce to the well known results $c_{ij}(\mathbf{x}^0) = \frac{1}{2}\delta_{ij}$ and $c_{ijkl}(\mathbf{x}^0) = \frac{1}{2}\delta_{ik}\delta_{jl}$. Otherwise, $\mathbf{x}^0$ lies on an edge or corner formed by two or more elements $\delta S^{(e)}$ $(e = 1, 2, \ldots)$ on S, each of which has two unit vectors $\mathbf{p}^{(e)}$ and $\mathbf{q}^{(e)}$ tangent to its line edges at $\mathbf{x}^0$. A list of these edge tangent vectors for the point $\mathbf{x}^0$ is accumulated over all such elements $\delta S^{(e)}$, and may be used to define explicitly the domain S_ε in terms of the polar co-ordinates.

The domain of integration S_ε may be considered to be composed of a number of contributions associated with the elements $\delta S^{(e)}$ adjacent to $\mathbf{x}^0$, each consisting of a spherical triangle with vertices P and Q corresponding to the two edge tangent vectors $\mathbf{p}^{(e)}$ and $\mathbf{q}^{(e)}$, along with the pole $\theta = 0$, as illustrated in Figure 3. When expressed in terms of spherical polar co-ordinates (r, θ, ϕ), the vertices P and Q are given by the angular co-ordinates (θ^p, ϕ^p) and (θ^q, ϕ^q), respectively. Then, each elemental domain is represented by a quadrilateral in (θ, ϕ) space bounded by $\theta = 0$, $\phi = \phi^p$, $\phi = \phi^q$ and a spherical geodesic of the form $\cos(\phi - \beta) = \tan\alpha/\tan\theta$ connecting (θ^p, ϕ^p) to (θ^q, ϕ^q), where α and β are parameters determined from the angular co-ordinates ϕ^p, ϕ^q, θ^p, θ^q. Integration over each of these (θ, ϕ) quadrilaterals is performed numerically using Gauss quadrature in terms of co-ordinates $-1 \leqslant \eta_1 \leqslant +1$ and $-1 \leqslant \eta_2 \leqslant +1$, by way of bilinear blending functions[18] that exactly interpolate into the interior of the quadrilateral the following edge functions:

$$\begin{aligned}
&\text{on } \eta_1 = -1, \quad \phi = \phi^p \quad \text{and} \quad \theta = \tfrac{1}{2}(\eta_2 + 1)\theta^p \\
&\text{on } \eta_1 = +1, \quad \phi = \phi^q \quad \text{and} \quad \theta = \tfrac{1}{2}(\eta_2 + 1)\theta^q \\
&\text{on } \eta_2 = -1, \quad \phi = \phi^p + \tfrac{1}{2}(\eta_1 + 1)(\phi^q - \phi^p) \quad \text{and} \quad \theta = 0 \\
&\text{on } \eta_2 = +1, \quad \phi = \phi^p + \tfrac{1}{2}(\eta_1 + 1)(\phi^q - \phi^p) \quad \text{and} \quad \cos(\phi - \beta) = \tan\alpha/\tan\theta
\end{aligned} \tag{67}$$

The resulting transformation functions, $\theta \equiv \theta(\eta_1, \eta_2)$ and $\phi \equiv \phi(\eta_1, \eta_2)$, are used to convert the surface integrals (65) and (66) into sums of integrals over a bi-unit square in a way analogous to the standard method for quadrature over boundary elements. When evaluating the coefficients numerically, it is found that 12 Gauss quadrature points for η_1 and 14 points for η_2 on each spherical triangle are sufficient to give 12 significant figures accuracy in $c_{ij}(\mathbf{x}^0)$, while 14 and 16 points, respectively, give similar accuracy in $c_{ijkl}(\mathbf{x}^0)$. Note that the coefficients c_{ijkl} are not generally of the form $c_{ik}\delta_{jl}$, as is sometimes assumed;[2,12] e.g. for the corner $x_1 + 2x_2 \leqslant 0$, $x_1 - 2x_2 \leqslant 0$, $x_3 \geqslant 0$, such as might be defined by three pairs of unit edge vectors $\mathbf{p}^{(e)}$, $\mathbf{q}^{(e)}$ taken two at a time from $(-2/\sqrt{5}, 1/\sqrt{5}, 0)$, $(-2/\sqrt{5}, -1/\sqrt{5}, 0)$, (0, 0, 1), it is found that $c_{1111} \approx 0{\cdot}2443$ and $c_{11} \approx 0{\cdot}1193$.

6. CONTRIBUTION FROM THE SURFACE S_*

The surface S_* is the part of $S(\varepsilon)$ between S_x and S_ε, and although its contribution to the BIE (11) vanishes as $\varepsilon \to 0$, its contribution to the BIDE (12) is in general non-zero. First, define the unit vectors $\hat{\mathbf{r}} \equiv \mathbf{r}/r$ and $\hat{\boldsymbol{\rho}} \equiv \boldsymbol{\rho}/\rho$. Then the part of S_* associated with an individual element, as illustrated by the area $PQQ'P'$ in Figure 1, is the region between the edge $\mathbf{r} = \varepsilon\hat{\boldsymbol{\rho}} - \frac{1}{2}\varepsilon^2\kappa(\psi)\mathbf{n}^0 + O(\varepsilon^3)$ of the curved surface δS_x and the edge $\mathbf{r} = \varepsilon\hat{\boldsymbol{\rho}}$ of the tangent plane δS_ρ, and it may be defined in terms of an extra off-plane angular co-ordinate $\omega \equiv \tan^{-1}(-\mathbf{n}^0 \cdot \hat{\mathbf{r}})$ to accompany the tangent plane polar co-ordinates ρ and ψ used earlier in Section 3. Then the domain S_* is composed from parts δS_* of the sphere $r = \varepsilon$ specified by $0 \leqslant \omega \leqslant \tan^{-1}(\frac{1}{2}\varepsilon\kappa(\psi) + O(\varepsilon^2)) = \frac{1}{2}\varepsilon\kappa(\psi) + O(\varepsilon^2)$ over some range $\psi_1 \leqslant \psi \leqslant \psi_2$ for each element that includes the source point and its contribution to the BIDE is of the form

$$I_{kl}(\mathbf{x}^0; S_*; \varepsilon) = \sum_{\text{elems}} \int_{\delta S_*} (\varepsilon^{-3}\hat{T}_{ikl}(\psi, \omega)u_i(\mathbf{x}^0) + O(\varepsilon^{-2}))\varepsilon^2 \cos\omega \, \mathrm{d}\omega \, \mathrm{d}\psi$$

$$= u_i(\mathbf{x}^0) \sum_{\text{elems}} \int_{\psi_1}^{\psi_2} \lim_{\varepsilon \to 0} \left\{ \frac{1}{\varepsilon} \int_0^{\frac{1}{2}\varepsilon\kappa(\psi)} \hat{T}_{ikl}(\psi, \omega) \cos\omega \, \mathrm{d}\omega \right\} \mathrm{d}\psi + O(\varepsilon) \tag{68}$$

where $\hat{T}_{ikl}(\psi, \omega) \equiv \hat{T}_{ikl}(\mathbf{n})$ as in (62) with $\mathbf{n} = -\hat{\mathbf{r}}$ on S_*. Then since

$$\lim_{\varepsilon \to 0} \left\{ \frac{1}{\varepsilon} \int_0^{\frac{1}{2}\varepsilon\kappa(\psi)} f(\psi, \omega) \, \mathrm{d}\omega \right\} = \tfrac{1}{2}\kappa(\psi) f(\psi, 0) \tag{69}$$

(68) reduces to the form (21) with

$$\mathrm{d}_{ikl}(\mathbf{x}^0) = \frac{1}{2} \sum_{\text{elems}} \int_{\psi_1}^{\psi_2} \kappa(\psi) \hat{T}_{ikl}(\psi, 0) \, \mathrm{d}\psi \tag{70}$$

which may be expressed as a sum of line integrals on the plane-projected surface elements δS_ρ. Notice that the contribution from S_* is zero if all the elements that include $\mathbf{x}^0$ are flat, i.e. $\kappa(\psi) = 0$. The contribution is also zero if $\mathbf{x}^0$ is on a smoothly curved part of the boundary (i.e. away from any geometric edges or corners), since all projected elements δS_ρ lie in the same plane $0 \leqslant \psi \leqslant 2\pi$, the curvature is symmetric about $\mathbf{x}^0$, i.e. $\kappa(\psi) = \kappa(\psi \pm \pi)$, and the kernel function is antisymmetric, i.e. $\hat{T}_{ikl}(\psi, 0) = -\hat{T}_{ikl}(\psi \pm \pi, 0)$.

7. THE TRACTION BOUNDARY INTEGRAL EQUATION (TBIE)

When the integrals over the component surfaces S_ε, S_* and S_x are reduced as described above and assembled into the BIDE, the following form is obtained:

$$C_{ijkl}u^0_{i,j} = -d_{ikl}u^0_i + \sum_p \{G_{ikl}(p)t_i(p) - H_{ikl}(p)u_i(p)\} \equiv W_{kl} \tag{71}$$

where the indices p refer to nodal values. The free-term coefficients C_{ijkl} are composed of the terms c_{ijkl} (65) which arise from the infinitesimal surface S_ε, incorporating the local geometry of the tangent planes at the source point, and terms that occur as coefficients of $u^0_{i,j}$ in (40) and (41) from using the special interpolations (24) and (25) on boundary elements near the source point. The coefficients d_{ikl} (70) arise from the infinitesimal surface S_*, and are non-zero only when the elements adjoining the source point have different curvature. Inverse coefficients C'_{klmn} are defined by the relationship $C'_{klmn}C_{ijkl} = \delta_{mi}\delta_{nj}$, and may be computed in terms of the inverse of a 9×9 matrix composed of the coefficients C_{ijkl}. Then the displacement derivatives are given by

$$u^0_{m,n} = C'_{klmn}W_{kl} \tag{72}$$

and the stress at $\mathbf{x}^0$ is

$$\sigma^0_{ij} = E_{ijmn}u^0_{m,n} = E_{ijmn}C'_{klmn}W_{kl} \tag{73}$$

where E_{ijmn} is given by (23). The formula (73) may be used to evaluate surface stresses from boundary element solutions. Values of traction at $\mathbf{x}^0$ on any one of the adjoining elements may be obtained as

$$t^{(e)}_i = n^{(e)}_j \sigma^0_{ij} = F^{(e)}_{ikl}W_{kl} \tag{74}$$

where

$$F^{(e)}_{ikl} = n^{(e)}_j E_{ijmn}C'_{klmn} \tag{75}$$

and superscript (e) denotes a quantity evaluated at $\mathbf{x}^0$ on the element e.

It is possible to construct separate TBIEs (74) for each of the differently orientated elements at a corner source point. However, none of these equations alone is satisfactory as a TBIE for general problems, since each is heavily biased towards one traction vector at the expense of the others. For a general formulation, the equations corresponding to each of these elements must be combined into a unique TBIE that incorporates all corner traction values in an algebraically balanced way. The contribution to this unique TBIE from each element should account for the fact that any such element may be subdivided into two nominal elements, the contributions from which should sum to the original amount. This additive property requires that the elemental contributions to the unique TBIE must be weighted into proportion to the angle subtended by the element at the source corner point.

Combining traction equations (74) in this way, the BIDE (71) is eventually reduced to the unique vector equation

$$\sum_e \{\psi^{(e)}t^{(e)}_i\} = \sum_e \{\psi^{(e)}n^{(e)}_j\}\sigma^0_{ij} = F_{ikl}W_{kl} \tag{76}$$

where

$$F_{ikl} \equiv \sum_e \{\psi^{(e)}F^{(e)}_{ikl}\} = \sum_e \{\psi^{(e)}n^{(e)}_j\}E_{ijmn}C'_{klmn} \tag{77}$$

and $\psi^{(e)}$ is the angle subtended by the boundary element e at $\mathbf{x}^0$. This equation will be referred to as the Traction Boundary Integral Equation (TBIE), due to the traction free terms, and it may be

used to obtain linear elastic solutions in the same way as the conventional displacement Boundary Integral Equation (BIE). In the special case where the source point lies on a smooth part of the boundary with smoothly varying displacement, the free-term coefficients are of the form $C_{ijkl}(\mathbf{x}^0) = c_{ijkl}(\mathbf{x}^0) = \frac{1}{2}\delta_{ik}\delta_{jl}$, $d_{ikl} = 0$, the normal vector $\mathbf{n}^{(e)}$ is unique, and the TBIE (76) reduces to the well-known form[1,2,5,12]

$$\tfrac{1}{2}t_i^0 = n_j^0 E_{ijkl} \sum_p \{G_{mkl}(p)t_m(p) - H_{mkl}(p)u_m(p)\} \tag{78}$$

8. DUAL EQUATIONS FOR CRACK PROBLEMS

The simplest strategy for modelling general fracture problems using the boundary element method involves arranging identical meshes of elements on each crack surface. Then dual nodes exist at points on the crack, at which both the displacement equation BIE and the traction equation TBIE may be applied. An exception to this arises for the unique nodes on the crack front, where only the displacement equation is applied. For these crack front source points, the free-term coefficients $c_{ij}(\mathbf{x}^0)$ may be determined from the definition of S_ε described in Section 5, except that contributions from the elements on the crack surfaces are excluded from the list of edge tangent vectors $\mathbf{p}^{(e)}$ and $\mathbf{q}^{(e)}$. For a crack front point that does not also lie on a non-crack surface, this reduces to $c_{ij}(\mathbf{x}^0) = \delta_{ij}$ as for an interior point.

Denoted opposite crack surfaces by S^+ and S^-, and the remainder of the boundary S by $\bar{S}$. The case where $\mathbf{x}^0$ is not on a crack is quite straightforward and equations are set up as for a non-crack problem. When $\mathbf{x}^0$ is on a crack, the free terms must be organized so as to generate a balanced set of equations. Let the indices p and q refer to nodal points on the surface $\bar{S}$ and on the crack, respectively. Since the normal vectors on each coincident pair of elements on the crack surfaces are mutually opposite $\mathbf{n}^+(\mathbf{x}) = -\mathbf{n}^-(\mathbf{x})$, the coefficients $H_{ij}^{\pm}(q)$, $H_{ikl}^{\pm}(q)$, $G_{ij}^{\pm}(q)$ and $G_{ikl}^{\pm}(q)$ associated with integrals taken over the respective surfaces $S^{\pm}$ satisfy

$$\begin{aligned} H_{ij}^{+}(q) &= -H_{ij}^{-}(q), \quad G_{ij}^{+}(q) = G_{ij}^{-}(q) \\ H_{ikl}^{+}(q) &= -H_{ikl}^{-}(q), \quad G_{ikl}^{+}(q) = G_{ikl}^{-}(q) \end{aligned} \tag{79}$$

Then, grouping the terms $d_{ikl}^{\pm}$ (70) with the other displacement coefficients $H_{ikl}^{\pm}$ for notational convenience, the BIE and the BIDE are of the form

$$\begin{aligned} c_{ij}^{+}(\mathbf{x}^0)u_i^{+}(\mathbf{x}^0) + c_{ij}^{-}(\mathbf{x}^0)u_i^{-}(\mathbf{x}^0) = &\sum_p \{G_{ij}(p)t_i(p) - H_{ij}(p)u_i(p)\} \\ &+ \sum_q \{G_{ij}^{+}(q)[t_i^{+}(q) + t_i^{-}(q)] \\ &- H_{ij}^{+}(q)[u_i^{+}(q) - u_i^{-}(q)]\} = W_j \end{aligned} \tag{80}$$

$$\begin{aligned} C_{ijkl}^{+}(\mathbf{x}^0)u_{i,j}^{+}(\mathbf{x}^0) + C_{ijkl}^{-}(\mathbf{x}^0)u_{i,j}^{-}(\mathbf{x}^0) = &\sum_p \{G_{ikl}(p)t_i(p) - H_{ikl}(p)u_i(p)\} \\ &+ \sum_q \{G_{ikl}^{+}(q)[t_i^{+}(q) + t_i^{-}(q)] \\ &- H_{ikl}^{+}(q)[u_i^{+}(q) - u_i^{-}(q)]\} = W_{kl} \end{aligned} \tag{81}$$

Note that nodes where a crack intersects a non-crack surface give contributions to both lists p and q.

It can be seen that the BIDE (81) is deficient in the quantities $(u_i^{+}(q) + u_i^{-}(q))$, which are represented only in the free terms of the BIE. Similarly, the BIE (80) contains no information

about the crack pressure $(t_i^+(q) - t_i^-(q))$, and neither does the right-hand side of the BIDE. This accounts for the inability of the BIE alone to model cracks with applied traction boundary conditions, and indicates the form which the TBIE should ideally adopt. For an algebraically complete representation of the crack problem, the free terms in the TBIE defined from the BIDE must involve the quantities $(t_i^+(q) - t_i^-(q))$. In terms of the displacement derivatives, the traction sum and difference are

$$t_i^+ \mp t_i^- = \sigma_{ij}^+ n_j^+ \mp \sigma_{ij}^- n_j^- = n_j^+ (\sigma_{ij}^+ \pm \sigma_{ij}^-) = n_j^+ E_{ijkl}(u_{k,l}^+ \pm u_{k,l}^-) \tag{82}$$

and so it is necessary to reorganize the BIDE to ensure that free terms $(u_{k,l}^+ + u_{k,l}^-)$ are produced. Define the symmetric $s_{klmn} = \frac{1}{2}(C_{klmn}^+ + C_{klmn}^-)$ and antisymmetric $a_{klmn} = \frac{1}{2}(C_{klmn}^+ - C_{klmn}^-)$ combinations of the free-term coefficients, along with the symmetric inverse $\bar{s}_{mnpq}$, defined by $\bar{s}_{mnpq} s_{klmn} = \delta_{pk}\delta_{ql}$. Then, the emergence of the required combination of displacement derivatives at the source position can be guaranteed by the operation

$$\bar{s}_{mnpq}(C_{klmn}^+ u_{k,l}^+ + C_{klmn}^- u_{k,l}^-) = (u_{p,q}^+ + u_{p,q}^-) + \bar{s}_{mnpq} a_{klmn}(u_{k,l}^+ - u_{k,l}^-) \tag{83}$$

Thus, defining the operator

$$F_{mkl} = \sum_e \{\psi^{(e)} n_f^{(e)+}\} E_{mfgh} \bar{s}_{klgh} \tag{84}$$

analogous to (77) except that the summation range covers only those elements e on the crack surface S^+ that include the source point $\mathbf{x}^0$, the BIDE (81) is transformed into the following traction equation:

$$\sum_e \{\psi^{(e)}(t_m^{(e)+}(\mathbf{x}^0) - t_m^{(e)-}(\mathbf{x}^0))\} + F_{mkl} a_{ijkl}(u_{i,j}^+(\mathbf{x}^0) - u_{i,j}^-(\mathbf{x}^0)) = F_{mkl} W_{kl} \tag{85}$$

Taking the summation range in equations (84) and (85) over crack elements only, rather than over all elements as in (76) and (77), ensures the emergence of an algebraically balanced combination of strong crack pressure terms in the TBIE when $\mathbf{x}^0$ is at the intersection of a crack and a non-crack surface.

In the general problem, a complete solution for displacement and traction on both crack surfaces is supplied by applying the two equations BIE and TBIE together at source points on the crack locus. In many cases however, the crack faces have specified traction boundary conditions, and solutions for the opening displacement $(u_i^+(q) - u_i^-(q))$ over the interior of a crack may be obtained using only the TBIE at source points on the crack locus. Source points where a crack intersects with an exterior boundary always require two equations, since the contributions from the non-crack boundary in (81) are not only in the combination $(u_i^+(p) - u_i^-(p))$.

When the source point $\mathbf{x}^0$ lies on a smooth crack surface with smoothly varying displacement, the coefficients $C_{ijkl}^+(\mathbf{x}^0)$ and $C_{ijkl}^-(\mathbf{x}^0)$ are identical, $C_{ijkl}^+(\mathbf{x}^0) = c_{ijkl}^+(\mathbf{x}^0) = C_{ijkl}^-(\mathbf{x}^0) = c_{ijkl}^-(\mathbf{x}^0) = \frac{1}{2}\delta_{ik}\delta_{jl}$, and so the antisymmetric contribution to the TBIE (85) is $a_{ijkl} = 0$. Consequently, the nine symmetric displacement derivative equations (81) may be reduced to three equations in which the only free term is the crack surface traction difference, and this is the form of the traction vector equation that is usually presented for crack problems[1,2]

$$\begin{aligned}\tfrac{1}{2}(t_m^+(\mathbf{x}^0) - t_m^-(\mathbf{x}^0)) = {} & n_g^+ E_{mgkl} \sum_p \{G_{ikl}(p) t_i(p) - H_{ikl}(p) u_i(p)\} \\ & + n_g^+ E_{mgkl} \sum_q \{G_{ikl}^+(q)[t_i^+(q) + t_i^-(q)] \\ & - H_{ikl}^+(q)[u_i^+(q) - u_i^-(q)]\}\end{aligned} \tag{86}$$

However, it is not generally possible to construct a TBIE in which all the displacement derivative terms have been eliminated. In this case, it is necessary to find accurate numerical approximations for the derivatives of displacement occurring explicitly in equation (85) in terms of displacement and traction on the boundary. Simply calculating displacement derivatives from the usual isoparametric representations (15) on one arbitrarily chosen boundary element is generally inadequate, and full use must be made of all information available.

9. ESTIMATION OF SURFACE DISPLACEMENT GRADIENTS

A successful boundary element method for general crack problems based on the TBIE depends upon the accuracy with which the residual displacement derivatives in (85) are estimated. For an optimal estimate applicable to any corner geometry and loading, full use of all available surface traction values must be made, since these contain direct information about the displacement derivatives. When calculating displacement derivatives by way of stress values from surface tractions, it is possible to use a maximum of only three differently orientated elements. Therefore, if information from more than three corner elements is to be fully utilized in a unique general formula, then an average will be required in which the contribution from each element is weighted appropriately. There arise three distinct basic cases, described in (a)–(c) below, from which the general case is developed for a corner comprising several boundary elements. The procedure in each case involves the definition of nine simultaneous linear equations in the nine required displacement derivatives $u^0_{i,j}$, each equation representing some information valid at $\mathbf{x}^0$. The set of nine equations is solved numerically to give $u^0_{i,j}$ in terms of nodal values of traction and displacement.

(a) *The point* $\mathbf{x}^0$ *is on an element that is on a smooth part of the surface, i.e., not at an edge or a corner.* Define orthonormal base vectors $\mathbf{a}^0$, $\mathbf{b}^0$, $\mathbf{n}^0$ corresponding to two tangent vectors and the normal to the element at $\mathbf{x}^0 = \mathbf{x}(\xi^0)$. The traction components ($i = 1, 2, 3$) give

$$n^0_j E_{ijkl} u^0_{k,l} = \bar{t}_i(\xi^0) \tag{87}$$

where E_{ijkl} is defined in (23), and $\bar{t}_i(\xi)$ is the usual traction interpolation (15). The tangential derivatives of displacement ($i = 1, 2, 3$) give

$$\begin{aligned} a^0_j u^0_{i,j} &= a^0_j \bar{u}_{i,j}(\xi^0) \\ b^0_j u^0_{i,j} &= b^0_j \bar{u}_{i,j}(\xi^0) \end{aligned} \tag{88}$$

where $\bar{u}_{i,j}(\xi^0)$ are defined as in (26) from the displacement interpolation (15).

(b) *The point* $\mathbf{x}^0$ *is on an edge comprising two differently orientated surface elements.* Define orthonormal base vectors $\mathbf{a}^e, \mathbf{b}^e, \mathbf{n}^e$, corresponding to two tangent and one normal to each element e ($= 1, 2$) at $\mathbf{x}^0 = \mathbf{x}(\xi^e)$, such that $\mathbf{a}^1 = \mathbf{a}^2 = \mathbf{a}$ is along the common edge. The normal components of traction on the two elements ($e = 1, 2$) give

$$n^e_i n^e_j E_{ijkl} u^0_{k,l} = n^e_i \bar{t}_i(\xi^e) \tag{89}$$

and the shear stress acting perpendicular to the edge gives

$$n^1_i n^2_j E_{ijkl} u^0_{k,l} = \tfrac{1}{2}(n^1_i \bar{t}_i(\xi^2) + n^2_i \bar{t}_i(\xi^1)) \tag{90}$$

Ideally, the two combinations $n^1_i \bar{t}_i(\xi^2)$ and $n^2_i \bar{t}_i(\xi^1)$ occurring on the right-hand side of (90) should represent the same stress component; however, numerical traction solutions will not

necessarily satisfy this condition and so the two values are averaged to give a symmetric formulation. The two shear tractions acting parallel to the common edge give

$$\begin{aligned} a_i n_j^1 E_{ijkl} u_{k,l}^0 &= a_i \bar{t}_i(\xi^1) \\ a_i n_j^2 E_{ijkl} u_{k,l}^0 &= a_i \bar{t}_i(\xi^2) \end{aligned} \tag{91}$$

Displacement gradients along the common edge ($i = 1, 2, 3$) give

$$a_j u_{i,j}^0 = a_j \bar{u}_{i,j}(\xi^e) \tag{92}$$

where e may be taken to be either 1 or 2, and the rotation about the edge gives

$$(b_i^1 b_j^2 - b_i^2 b_j^1) u_{i,j}^0 = b_i^1 b_j^2 \bar{u}_{i,j}(\xi^2) - b_i^2 b_j^1 \bar{u}_{i,j}(\xi^1) \tag{93}$$

(c) *The point* $\mathbf{x}^0$ *is at a corner comprising three differently orientated surface elements.* Define orthonormal base vectors $\mathbf{a}^e$, $\mathbf{b}^e$, $\mathbf{n}^e$, corresponding to two tangents and one normal to each of the three elements e (= 1, 2, 3) at $\mathbf{x}^0 = \mathbf{x}(\xi^e)$. The normal components of tractions on each element ($e = 1, 2, 3$) give

$$n_i^e n_j^e E_{ijkl} u_{k,l}^0 = n_i^e \bar{t}_i(\xi^e) \tag{94}$$

and the shear components give

$$\begin{aligned} n_i^1 n_j^2 E_{ijkl} u_{k,l}^0 &= \tfrac{1}{2}(n_i^1 \bar{t}_i(\xi^2) + n_i^2 \bar{t}_i(\xi^1)) \\ n_i^2 n_j^3 E_{ijkl} u_{k,l}^0 &= \tfrac{1}{2}(n_i^2 \bar{t}_i(\xi^3) + n_i^3 \bar{t}_i(\xi^2)) \\ n_i^3 n_j^1 E_{ijkl} u_{k,l}^0 &= \tfrac{1}{2}(n_i^3 \bar{t}_i(\xi^1) + n_i^1 \bar{t}_i(\xi^3)) \end{aligned} \tag{95}$$

which involve averaged values of traction as in (90). Rotation about the normal direction on each element ($e = 1, 2, 3$) gives

$$(a_i^e b_j^e - a_j^e b_i^e) u_{i,j}^0 = (a_i^e b_j^e - a_j^e b_i^e) \bar{u}_{i,j}(\xi^e) \tag{96}$$

An optimum estimate of displacement derivatives at a point $\mathbf{x}^0$ common to several elements should involve values of traction and displacement taken from all those elements. Furthermore, contributions from each element should be additive, by the same reasoning that leads to the averaged TBIE (76) . Consequently, a general formula for the estimation of displacement derivatives at the conjunction $\mathbf{x}^0$ of several boundary elements must necessarily involve contributions from each element weighted in accordance with the angle subtended by that element at $\mathbf{x}^0$. In the present method, the following algorithm is used to obtain estimates for the values of $u_{i,j}^0$ in terms of the three basic cases (a)–(c) above:

Consider in turn each element e that includes $\mathbf{x}^0$:

(i) Find the two edges $P^{(e)}$ and $Q^{(e)}$ that adjoin $\mathbf{x}^0$.
(ii) Compute unit tangent vectors $\mathbf{p}^{(e)}$ and $\mathbf{q}^{(e)}$ along $P^{(e)}$ and $Q^{(e)}$ at $\mathbf{x}^0$.
(iii) Calculate the angle $\psi^{(e)} = \cos^{-1}(\mathbf{p}^{(e)} \cdot \mathbf{q}^{(e)})$ subtended at $\mathbf{x}^0$.
(iv) Find any elements that share either of the edges $P^{(e)}$ or $Q^{(e)}$ and that have normal vector at $\mathbf{x}^0$ different from that on e; there will be none or one or two of such elements.
(v) Use procedure (a), (b) or (c) to obtain an estimate $u_{i,j}^0(e)$ of $u_{i,j}^0$ associated with element e, in terms of the tractions and displacements on e and its immediate neighbours if any.

From this list, accumulate the average of all such estimates according to

$$u^0_{i,j} = \sum_e \{\psi^{(e)} u^0_{i,j}(e)\} \Big/ \sum_e \{\psi^{(e)}\} \tag{97}$$

and this is the balanced estimate to be used in the TBIE (85).

10. NUMERICAL RESULTS

The main objective of developing a numerical representation for the TBIE is its application to crack problems. Three example crack problems are described below, for which complete numerical solutions have been obtained from the dual equations, BIE (80) and TBIE (85), applied on the crack locus. The elastic constants of all examples are chosen to be $E = 71{\cdot}0$ (GPa) and $\nu = 0.3$, and either quadrilateral nine-noded or triangular six-noded continuous quadratic isoparametric boundary elements are used on all surfaces. Quarter point elements are used along the crack front, and values of stress intensity factor are derived from the displacement solution on the crack faces as follows:[6] the stress intensity factors at a point $\xi = (\xi^0_1, -1)$ on the crack front $\xi_2 = -1$ of a quadrilateral quarter point element $-1 \leqslant \xi_\alpha \leqslant +1$ are

$$\begin{aligned} K_I &= k\mathbf{A}\cdot\hat{\mathbf{n}}, \\ K_{II} &= k\mathbf{A}\cdot\hat{\mathbf{q}} \\ K_{III} &= (1-\nu)k\mathbf{A}\cdot\hat{\mathbf{p}} \end{aligned} \tag{98}$$

where $\mathbf{A} = \frac{1}{3}\{8\boldsymbol{\Delta}(\xi^0_1, 0) - \boldsymbol{\Delta}(\xi^0_1, +1)\}$ and $\boldsymbol{\Delta} = \mathbf{u}^+ - \mathbf{u}^-$ is the relative displacement between the two crack faces evaluated at the quarter point node $(\xi^0_1, 0)$ and the node $(\xi^0_1, +1)$ furthest from the crack front $(\xi^0_1, -1)$, $\hat{\mathbf{n}}$ is the unit outward normal on the crack surface S^- at the crack front, $\hat{\mathbf{p}}$ is a unit vector tangent to the crack front, $\hat{\mathbf{q}}$ is a unit vector orthogonal to both $\hat{\mathbf{n}}$ and $\hat{\mathbf{p}}$, $\mathbf{L} = \mathbf{x}(\xi^0_1, +1) - \mathbf{x}(\xi^0_1, -1)$, and $k = [E/8(1-\nu^2)]\sqrt{2\pi/(\mathbf{L}\cdot\hat{\mathbf{q}})}$.

Before considering the crack examples, there are two observations, (i) and (ii) below, to be made concerning the convergence of the TBIE in the present formulation.

(i) The TBIE alone may be used instead of the BIE to solve non-crack problems, and such solutions provide a useful test of the validity of the present formulation. If the conventional interpolations (15) are used instead of the special interpolations (24) and (25), solutions to the hypersingular TBIE do not in general converge. Test cases which have exact solutions that can be described reasonably well using the assumed elemental interpolations (15), such as a cube under uniform tension, shear or bending with a mesh of regular boundary elements, give quite acceptable results. However, such simple problems do not test the ability of the present numerical method to produce inexact results that converge to the correct solution. For test cases in which (15) cannot closely represent the exact solution, such as a solid cylinder under axial torsion with a coarse mesh of boundary element, if is found that numerical solutions of the hypersingular TBIE are wildly inaccurate and do not improve as the number of elements is increased. On the other hand, the special interpolation scheme, (24) and (25), consistently produces reasonable solutions which are of comparable accuracy to those from the BIE and which approach the exact solution as more elements are used.

(ii) In cases involving very coarse meshes of boundary elements, the choice of the localising function $\bar{N}(\xi)$, (27), used in the regularization of the assumed forms for the displacement and traction, (24) and (25), can make a considerable difference to numerical solutions of the TBIE. However, as more boundary elements are used, it is found that the influence of the

choice of $\bar{N}(\xi)$ diminishes and solutions to the TBIE converge uniformly. In this respect, the use of different $\bar{N}(\xi)$ is analogous to using different types of boundary elements to obtain discrete nodal solutions, all of which converge to the same result. The simplest choice is to define $\bar{N}(\xi)$ as the interpolation function associated with the source node on the element, and this is used in all the cases below.

10.1. Inclined circular crack in an infinite solid

This is a standard test case for numerical analyses of three-dimensional crack problems, since it admits a closed-form solution. Consider a circular crack of radius a centred at the origin (0, 0, 0) of co-ordinates and lying in the plane $x_2 \sin\omega + x_3 \cos\omega = 0$. The surfaces of the crack are loaded by tractions $t_2 = \pm \sigma \sin\omega$, and the stress intensity factors are identical to those for the case of remote uniaxial tension $\sigma_{22} = \sigma$ given by[19]

$$K_I = 2\sigma\sqrt{\frac{a}{\pi}}\sin^2\omega$$

$$K_{II} = 2\sigma\sqrt{\frac{a}{\pi}}\left(\frac{2}{2-\nu}\right)\cos\omega\sin\omega\cos\phi \tag{99}$$

$$K_{III} = 2\sigma\sqrt{\frac{a}{\pi}}\left(\frac{2-2\nu}{2-\nu}\right)\cos\omega\sin\omega\sin\phi$$

where $\phi = \cos^{-1} r_1/a$ is an angular co-ordinate for a point (r_1, r_2, r_3) on the crack front. The specific example considered is an inclined crack of unit radius $a = 1{\cdot}0$, lying in the plane $x_2 + x_3 = 0$ ($\omega = 45°$), and loaded by traction $t_2 = \pm\sqrt{\frac{1}{2}}$; this is a mixed-mode problem involving all three stress intensity factors K_I, K_{II} and K_{III}.

Three different meshes of continuous boundary elements are considered to illustrate the convergence of the results. The mesh on each crack face involves N_R regular subdivisions in the radial direction, and N_A regular subdivisions of each quadrant in the angular ϕ-direction. Mirror symmetry about the plane $x_1 = 0$ is exploited to halve the number of elements, thereby considerably reducing the size of the numerical problem. The meshes considered are defined as follows: mesh A is $N_A = 2$, $N_R = 2$; mesh B is $N_A = 4$, $N_R = 2$; mesh C is $N_A = 4$, $N_R = 4$. Mesh A is illustrated in Figure 4.

Results for the 45° inclined crack are shown in Table I, where values of stress intensity factor (98) obtained using the three element meshes are given at 22·5° intervals around the crack front. The largest error in any of the values of stress intensity factor is about 0·4 per cent from mesh A, about 0·3 per cent from mesh B and about 0·2 per cent from mesh C.

10.2. Circumferential crack in a cylinder under tension

This edge-crack example involves a solid cylinder of radius R and length $2L$, defined by the region $\{x_1^2 + x_2^2 \leqslant R^2,\ -L \leqslant x_3 \leqslant +L\}$, with a circumferential crack of depth a lying in the annular region $x_3 = 0$, $R - a \leqslant \{x_1^2 + x_2^2\}^{1/2} \leqslant R$. The ends $x_3 = \pm L$ are loaded in tension by unit tractions $t_2 = \pm\sigma$ ($\sigma = 1$). Two crack lengths of $a/R = 0{\cdot}5$ and 0·9 are studied, with the dimensions $R = 1{\cdot}0$ and $L = 4{\cdot}0$ chosen to simulate an infinitely long cylinder. The known solution[19] for an infinitely long cylinder with $a/R = 0{\cdot}5$ is $K_I/\sigma\sqrt{\pi a} = 1{\cdot}940 \pm 0{\cdot}1$ per cent,

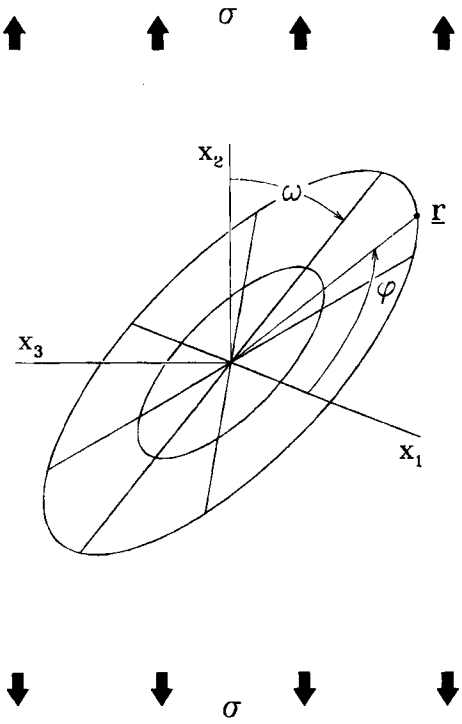

Figure 4. Inclined circular crack in an infinite solid under remote uniaxial tension

Table I. Stress intensity factors around a 45° inclined circular crack using three different boundary element meshes A, B and C

	ϕ	0·0°	22·5°	45·0°	67·5°	90·0°
	K_I	0·5636	0·5624	0·5636	0·5624	0·5636
A	K_{II}	$<10^{-12}$	0·2529	0.4678	0.6105	0.6616
	K_{III}	0·4653	0·4288	0·3290	0·1776	0·0000
	K_I	0·5638	0·5638	0·5638	0·5638	0·5638
B	K_{II}	$<10^{-12}$	0·2533	0·4681	0·6116	0·6620
	K_{III}	0·4656	0·4302	0·3292	0·1782	0·0000
	K_I	0·5636	0·5636	0·5636	0·5636	0·5636
C	K_{II}	$<10^{-12}$	0·2536	0·4687	0·6124	0·6628
	K_{III}	0·4644	0·4291	0·3284	0·1777	0·0000
	K_I	0·5642	0·5642	0·5642	0·5642	0·5642
exact	K_{II}	0·0000	0·2540	0·4694	0·6133	0·6638
	K_{III}	0·4646	0·4293	0·3285	0·1778	0·0000

giving $K_I = 2{\cdot}431$ (± 0.003), and that with $a/R = 0{\cdot}9$ is $K_I/\sigma\sqrt{\pi a} = 16{\cdot}67 \pm 0.1$ per cent, giving $K_I = 28{\cdot}03$ ($\pm 0{\cdot}03$).

For the case $a/R = 0{\cdot}5$, a symmetric mesh of boundary elements is used comprising eight regular subdivisions in the angular direction $0 \leqslant \phi \leqslant 2\pi$, ten subdivisions of the length

$-L \leqslant x_3 \leqslant L$ weighted in the ratios 20:10:5:3:2:2:3:5:10:20, and two equal subdivisons of the crack in the radial direction. Mirror symmetry about the planes $x_1 = 0$ and $x_2 = 0$ is exploited to reduce the number of elements by a factor of four. For this mesh, the values of stress intensity factor (98) alternate between $K_I = 2{\cdot}419$ and $2{\cdot}423$ all along the crack front, corresponding to an error of about 0·5 per cent with $K_{II} \sim 10^{-4}$ and $K_{III} \sim 10^{-9}$. With a mesh composed of 12 lengthways subdivisons in the ratio 20:10:5:3:2:1:1:2:3:5:10:20 and four equal radial subdivisions on the crack, the stress intensity factor varies between $K_I = 2{\cdot}440$ and $2{\cdot}439$, amounting to an error of about 0·4 per cent with $K_{II} \sim 10^{-5}$ and $K_{III} \sim 10^{-9}$ all along the crack front. For the case $a/R = 0{\cdot}9$, a similar mesh is used, with ten subdivisions of the length $-L \leqslant x_3 \leqslant +L$ weighted in the ratios 20:10:5:3:2:2:3:5:10:20, and four equal subdivisions of the crack in the radial direction. For this mesh, the values of stress intensity factor alternate between $K_I = 28{\cdot}09$ and $28{\cdot}12$ all along the crack front, corresponding to an error of about 0·3 per cent, with $K_{II} \sim 10^{-4}$ and $K_{III} \sim 10^{-9}$

10.3. Inclined straight edge crack in a large solid block under tension

A rectangular block $0 \leqslant x_1 \leqslant b$, $-b \leqslant x_2 \leqslant \frac{3}{2}b$, $-c \leqslant x_3 \leqslant c$ contains an inclined flat crack over the region $0 \leqslant x_1 \leqslant a\sin\omega$, $-c \leqslant x_3 \leqslant c$ of the inclined plane $x_1\cos\omega - x_2\sin\omega = 0$, with the crack front along $x_1 = a\sin\omega$, $x_2 = a\cos\omega$. The block is loaded in tension by tractions $t_2 = +\sigma$ on $x_2 = \frac{3}{2}b$ and $t_2 = -\sigma$ on $x_2 = -b$. In addition, a further constraint $u_3 = 0$ is imposed on $x_3 = \pm c$ to simulate a state of plane strain for comparison of results with known two-dimensional solutions.[20] Mirror symmetry about the plane $x_3 = 0$ is exploited to reduce the size of the problem by about one half. This inclined crack example is included to demonstrate the correct behaviour of the TBIE along the asymmetric double corner $x_1 = x_2 = 0$, where accurate evaluation of the free-term coefficients, (65) and (66), and a balanced form for the TBIE (85) are crucial. Although this example is essentially two dimensional, it does provide a useful test of the present three-dimensional numerical method. In the test cases, the loading is taken to be $\sigma = 1{\cdot}0$, the dimensions are chosen to be $a = 0{\cdot}5$, $b = 1{\cdot}0$, $c = 0{\cdot}25$, and two crack angles are considered, $\omega = 67{\cdot}5°$ and $\omega = 45{\cdot}0°$.

The mesh used consists of 72 boundary elements, and is illustrated in Figure 5. Nine-noded quadrilateral quarter point elements are used along the crack front, and six-noded triangular quarter point elements are clustered around the point $(a\sin\omega, a\cos\omega, c)$ where the crack front meets the surface $x_3 = c$. One element spans the half-thickness $0 \leqslant x_3 \leqslant c$, and the surface $x_3 = c$ is subdivided as follows: $0 \leqslant x_1 \leqslant a\sin\omega$ has four equal subdivisions; $a\sin\omega \leqslant x_1 \leqslant b$ has two subdivisions weighted 1:5 from the crack tip; the region between the crack and $x_2 = \frac{3}{2}b$ and the region $\{x_1 \geqslant a\sin\omega;\ a\cos\omega \leqslant x_2 \leqslant \frac{3}{2}b\}$ both have three subdivisions weighted 1:2:3 in the direction of increasing x_2; the region between the crack and $x_2 = -b$ and the region $\{x_1 \geqslant a\sin\omega;\ -b \leqslant x_2 \leqslant a\cos\omega\}$ both have three subdivisions weighted 1:2:3 in the direction of decreasing x_2.

The boundary element results are shown in Table II. For crack angle $\omega = 67.5°$, the stress intensity factors K_I and K_{II}, using (98), at the symmetry plane $x_3 = 0$ are with 1·0 per cent of the reference solution, while those for $\omega = 45{\cdot}0°$ are within 1·5 per cent. For both crack angles, the stress intensity factors vary along the crack front by less than 1·2 per cent, indicating that the inability of the triangular quarter point elements on the surface $x_3 = c$ to represent the multi-valued singular traction t_3 at the tip position $(a\sin\omega, a\cos\omega, c)$ has little influence on the accuracy of the stress intensity factors.

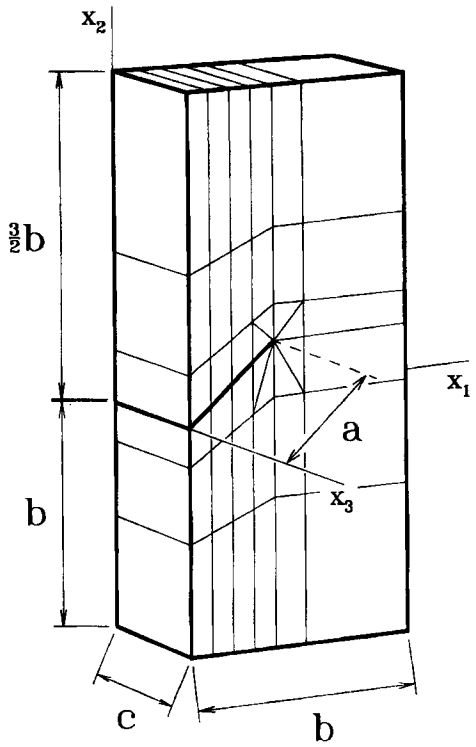

Figure 5. Inclined edge crack in a rectangular solid

Table II. Stress intensity factors for inclined edge cracks

ω	Solution	K_I	K_{II}	K_{III}
45·0°	$x_3/c = 0·0$	1·516	−0·730	0·000
	$x_3/c = 0·5$	1·517	−0·729	0·001
	$x_3/c = 1·0$	1·525	−0·730	0·000
	Reference 20 (2-D)	1·504	−0·739	0·000
67·5°	$x_3/c = 0·0$	2·857	−0·623	0·000
	$x_3/x = 0·5$	2·858	−0·621	0·001
	$x_3/c = 1·0$	2·889	−0·626	0·000
	Reference 20 (2-D)	2·845	−0·618	0·000

11. CONCLUSION

The aim of the present work is to develop a single-domain boundary element method for general three-dimensional elastostatic crack problems, including a complete numerical treatment of the TBIE.

The hypersingular BIDE for displacement derivatives at a general corner point on the boundary is developed from basic principles, involving a limiting procedure in which an infinitesimal spherical region around the source point is excluded from the volume. Three subdivisions of the boundary surface are defined and each contribution to the global equation is

considered separately. Apparent singularities arising from this artificial subdivision of the integration domain are deliberately excluded from the limiting form of the BIDE by reference to Hadamard principal values.

An investigation into the hypersingular nature of the BIDE for displacement derivatives on the boundary shows the conditions that must be satisfied by the surface solution in order to produce a valid numerical method. Suitable modifications of the assumed displacement and traction fields local to the source point are performed, using special interpolation functions, so that continuous boundary elements may be used in a numerical solution scheme.

The free-term coefficients of the displacement derivatives in the BIDE are computed directly in terms of integrals over spherical triangles, using a numerical procedure that can be applied to any corner geometry. Other contributions to the source node coefficients arise in the form of Hadamard principle value integrals, and these are evaluated numerically by reference to polar co-ordinates defined on the planes tangent to the elements at the source point.

A unique definition for the TBIE for non-crack problems is proposed from the BIDE for displacement derivatives, the free term of which comprises a balanced combination of traction values from all elements that include the source point. The forms of the BIE and the BIDE with the source point on the coincident surfaces of a crack is investigated, and a means of constructing a TBIE is given that ensures the emergence of strong crack pressure terms necessary for a robust numerical method. When applied to crack problems, the TBIE includes two sets of free terms, each involving tractions on the crack and residual displacement derivative terms. Accurate estimation of these residual displacement derivatives in terms of boundary element data is necessary for a successful treatment, and a simple algorithm for their computation is given.

Boundary element solutions to non-crack problems obtained from the hypersingular TBIE converge uniformly and are of comparable accuracy to those from the conventional BIE. However, numerical solutions of the hypersingular TBIE do not in general converge if the special interpolation is not used. Boundary element solutions are presented for mixed-mode problems involving internal or edge cracks. Quarter point elements are used along the crack fronts, and stress intensity factors are determined from the numerical displacement solutions on the crack surfaces. Stress intensity factors converge very rapidly, and results accurate to about 1 per cent may be obtained even with very coarse boundary element meshes.

APPENDIX I: CALCULATION OF TANGENTIAL DERIVATIVES AND ELEMENT CURVATURE

The projection of a point $\mathbf{r}$ on a smooth boundary element δS_x onto the plane δS_ρ, tangent to this element $\mathbf{r} = \mathbf{0}$, is

$$\boldsymbol{\rho} = \mathbf{r} - (\mathbf{r} \cdot \mathbf{n}^0)\mathbf{n}^0 \tag{100}$$

where $\mathbf{n}^0$ denotes the unit vector outwardly normal to the element at $\mathbf{r} = \mathbf{0}$. The position vector on the surface δS_x is of the form

$$\mathbf{r} = \boldsymbol{\rho} + (\tfrac{1}{2}\rho^2\kappa(\psi) + O(\rho^3))\mathbf{n}^0 \tag{101}$$

where $\kappa \equiv \kappa(\psi)$ is the curvature of the surface δS_x at $\mathbf{r} = \mathbf{0}$, so that

$$r^2 = \rho^2 + \tfrac{1}{4}(\kappa(\psi))^2\rho^4 + O(\rho^5) \tag{102}$$

The unit outward normal $\boldsymbol{\eta}$ at $\mathbf{r}$ is of the form

$$\boldsymbol{\eta} = \mathbf{n}^0 - \kappa\boldsymbol{\rho} + O(\rho^2) \tag{103}$$

and the curvature is given by

$$\kappa(\psi) = 2\lim_{r\to 0}\{\mathbf{r}\cdot\mathbf{n}^0/r^2\} = 2\lim_{r\to 0}\{-\mathbf{r}\cdot\mathbf{n}/r^2\} \tag{104}$$

Spatial co-ordinates $z_1 = \rho\cos\psi$ and $z_2 = \rho\sin\psi$ on the tangent plane δS_ρ may be defined as

$$z_\alpha \equiv \hat{\mathbf{q}}^{(\alpha)}\cdot\mathbf{r} = \hat{q}_k^{(\alpha)}\rho_k \tag{105}$$

where $\hat{\mathbf{q}}^{(\alpha)}$ are two constant mutually orthogonal unit vectors on δS_ρ. These tangential co-ordinates are related to the intrinsic co-ordinates ξ_α defined on δS_x by

$$\frac{\partial z_\alpha}{\partial \xi_\beta} = \hat{q}_k^{(\alpha)}\frac{\partial x_k}{\partial \xi_\beta} = \hat{q}_k^{(\alpha)}\sum_m x_k^{(m)}\frac{\partial N^{(m)}}{\partial \xi_\beta} \tag{106}$$

The inverse partial derivatives are calculated by way of the matrix equation

$$\begin{bmatrix} \dfrac{\partial\xi_1}{\partial z_1} & \dfrac{\partial\xi_1}{\partial z_2} \\ \dfrac{\partial\xi_2}{\partial z_1} & \dfrac{\partial\xi_2}{\partial z_2} \end{bmatrix} \equiv \begin{bmatrix} \dfrac{\partial z_1}{\partial\xi_1} & \dfrac{\partial z_1}{\partial\xi_2} \\ \dfrac{\partial z_2}{\partial\xi_1} & \dfrac{\partial z_2}{\partial\xi_2} \end{bmatrix}^{-1} = \frac{1}{Z}\begin{bmatrix} \dfrac{\partial z_2}{\partial\xi_2} & -\dfrac{\partial z_1}{\partial\xi_2} \\ -\dfrac{\partial z_2}{\partial\xi_1} & \dfrac{\partial z_1}{\partial\xi_1} \end{bmatrix} \tag{107}$$

where

$$Z = \frac{\partial z_1}{\partial\xi_1}\frac{\partial z_2}{\partial\xi_2} - \frac{\partial z_1}{\partial\xi_2}\frac{\partial z_2}{\partial\xi_1} = (\hat{q}_k^{(1)}\hat{q}_l^{(2)} - \hat{q}_k^{(2)}\hat{q}_l^{(1)})\frac{\partial x_k}{\partial\xi_1}\frac{\partial x_l}{\partial\xi_2} \neq 0 \tag{108}$$

Then tangential derivatives involving the three spatial co-ordinates ρ_i, which are necessarily constrained to the tangent plane δS_ρ, and partial derivatives with respect to the two intrinsic co-ordinates ξ_α are related by

$$\frac{\partial}{\partial\rho_j} \equiv \frac{\partial z_\alpha}{\partial\rho_j}\frac{\partial}{\partial z_\alpha} = \sum_\alpha \hat{q}_j^{(\alpha)}\frac{\partial\xi_\beta}{\partial z_\alpha}\frac{\partial}{\partial\xi_\beta} \tag{109}$$

and so

$$\rho_j\left(\frac{\partial}{\partial\rho_j}\right)^0 = z_\alpha\left(\frac{\partial\xi_\beta}{\partial z_\alpha}\right)^0\left(\frac{\partial}{\partial\xi_\beta}\right)^0 \tag{110}$$

where the superscript zero refers to quantities evaluated at $\mathbf{r} = \mathbf{0}$. This allows calculation of the $O(\rho)$ terms in series expansions for functions of the intrinsic co-ordinates, and in particular for the interpolation functions

$$N^{(m)}(\boldsymbol{\xi}) = N^{(m)}(\boldsymbol{\xi}^0) + \left(\frac{\partial N^{(m)}}{\partial\xi_\beta}\right)^0\sum_\alpha\left(\frac{\partial\xi_\beta}{\partial z_\alpha}\right)^0\hat{q}_j^{(\alpha)}\rho_j + O(\rho^2) \tag{111}$$

For notational simplicity, define the following

$$\Delta_{i\alpha} \equiv \frac{\partial x_i}{\partial\xi_\alpha}, \quad \Delta_{i\alpha\beta} \equiv \frac{\partial^2 x_i}{\partial\xi_\alpha\partial\xi_\beta}, \quad \nabla_{\alpha i} \equiv \frac{\partial\xi_\alpha}{\partial\rho_i} \equiv \sum_\beta\left(\frac{\partial\xi_\alpha}{\partial z_\beta}\right)^0\hat{q}_i^{(\beta)} \tag{112}$$

each of which may be calculated numerically. Then $(\Delta_{i\alpha})^0 n_i^0 = 0$, and the radial vector $\mathbf{r}$ in (104) may be expanded in powers of ρ giving

$$n_i^0 r_i = \tfrac{1}{2}[n_i^0(\Delta_{i\alpha\beta})^0(\nabla_{\alpha k})^0(\nabla_{\beta l})^0\hat{\rho}_k\hat{\rho}_l]\rho^2 + O(\rho^3) \tag{113}$$

where $\hat{\boldsymbol{\rho}} \equiv \hat{\boldsymbol{\rho}}(\psi) \equiv \boldsymbol{\rho}/\rho$ is a unit vector in the direction of the plane polar angle ψ. Then the curvature parameter $\kappa(\psi)$ may be calculated using the formula

$$\kappa(\psi) = n_i^0(\Delta_{i\alpha\beta})^0(\nabla_{\alpha k})^0(\nabla_{\beta l})^0\hat{\rho}_k\hat{\rho}_l \tag{114}$$

REFERENCES

1. V. Sladek, J. Sladek and J. Balas, 'Boundary integral formulation of crack problems', *ZAMM* **66**, 83–94 (1986).
2. H. K. Hong and J. T. Chen, 'Derivations of integral equations of elasticity', *ASCE J. Eng. Mech.*, **114**, 1028–1044 (1988).
3. M. Guiggiani, G. Krishnasamy, T. J. Rudolphi and F. J. Rizzo, 'A general algorithm for the numerical solution of hypersingular boundary integral equations', *ASME J. Appl. Mech.*, **59**, 604–614 (1992).
4. A. Portela, M. H. Aliabadi and D. P. Rooke, 'The dual boundary element method: effective implementation for crack problems', *Int. j. numer. methods eng.*, **33**, 1269–1287 (1992).
5. Y. Mi and M. H. Aliabadi, 'Dual boundary element method for three-dimensional fracture mechanics analysis', *Eng. Anal. Boundary Elements*, **10**, 161–171 (1992).
6. M. L. Luchi and S. Rizzuti, 'Boundary elements for three-dimensional elastic crack analysis', *Int. j. numer. methods eng.*, **24**, 2253–2271 (1987).
7. K. Takakuda, T. Koizumi and T. Shibuya, 'On integral equation methods for crack problems', *Bull JSME*, **28**(236), 217–224 (1985).
8. S. Guimaraes and J. C. F. Telles, 'On a critical appreciation of the hyper-singular boundary element formulation applied to fracture mechanics problems', in H. Pina and C. A. Brebbia (eds.), *Boundary Element Technology*, Vol. VIII. Computational Mechanics Publications, Southampton, 1993, pp. 241–251.
9. L. F. Martha, L. J. Gray and A. R. Ingraffea, 'Three-dimensional fracture simulation with a single-domain direct boundary element formulation', *Int. j. numer. methods eng.*, **35**, 1907–1921 (1992).
10. V. Sladek, J. Sladek and M. Tanaka, 'Numerical solution of nonsingular BIE for crack problems', in C. A. Brebbia, J. Dominguez and F. Paris (eds.), *Boundary Elements XIV, Vol. 2: Stress Analysis and Computational Aspects*, Computational Mechanics Publications, Southampton, 1992.
11. K. H. Muci-Kuchler and T. J. Rudolphi, 'A weakly singular formulation of traction and tangent derivative boundary integral equations in three dimensional elasticity', *Eng. Anal. Boundary Elements*, **11**, 195–201 (1993).
12. Q. Huang and T. A. Cruse, 'On the non-singular traction-BIE in elasticity', *Int. j. numer. methods eng.*, **37**, 2041–2072 (1994).
13. J. C. Lachat and J. O. Watson, 'Effective numerical treatment of boundary integral equations: a formulation for three-dimensional elastostatics', *Int. j. numer. methods eng.*, **10**, 991–1005 (1976).
14. T. A. Cruse, 'Numerical Solutions in three-dimensional elastostatics', *Int. J. Solids Struct.*, **5**, 1259–1274 (1969).
15. P. K. Bannerjee and R. Butterfield, *Boundary Element Methods in Engineering Science*, 1st edn. McGraw-Hill, Maidenhead, 1981.
16. K. Hayami and C. A. Brebbia, 'Quadrature methods for singular and nearly singular integrals in 3-D boundary element method', *Boundary Elements X, Vol. 1*, Computational Mechanics Press, pp. 237–264.
17. V. Mantic, 'A new formula for the C-matrix in the Somigliana identity', *J. Elasticity* **33**, 191–201 (1993).
18. O. C. Zienkiewicz and R. L. Taylor, *The Finite Element Method Vol. 1: Basic Formulation and Linear Problems*, 4th edn., McGraw-Hill, Maidenhead, 1989.
19. Y. Murakami (ed.), *Stress Intensity Factors Handbook, Vols. 1 and 2*, 1st edn, Pergamon, Oxford, 1987.
20. R. N. L. Smith and D. Della-Ventura, 'Boundary element superposition methods for mixed-mode fracture problems', in H. Pina and C. A. Brebbia (eds.), *Boundary Element Technology*, Vol. VIII, Computational Mechanics Publications, Southampton, 1993, pp. 277–285.